NUMERICAL SIMULATION OF ENHANCED OIL RECOVERY FROM POROUS FORMATIONS

by

Partha Pratim Mukherjee

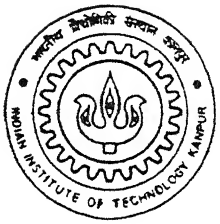

DEPARTMENT OF MECHANICAL ENGINEERING

INDIAN INSTITUTE OF TECHNOLOGY KANPUR

March, 1999

NUMERICAL SIMULATION OF ENHANCED OIL RECOVERY FROM POROUS FORMATIONS

A Thesis Submitted
In Partial Fulfilment of the Requirements
for the Degree of
Master of Technology

by

Partha Pratim Mukherjee

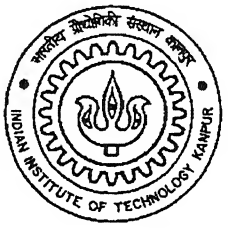

to the

DEPARTMENT OF MECHANICAL ENGINEERING
INDIAN INSTITUTE OF TECHNOLOGY KANPUR
INDIA

March, 1999

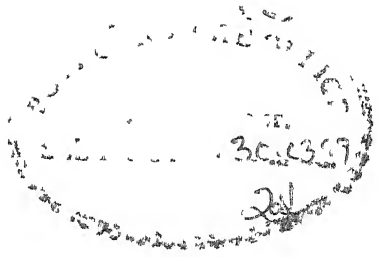

Certificate

It is certified that the work contained in the thesis entitled **Numerical Simulation of Enhanced Oil Recovery from Porous Formations** by Partha Pratim Mukherjee, has been carried out under my supervision and that this work has not been submitted elsewhere for a degree

Gautam Biswas

Gautam Biswas
Department of Mechanical Engineering
IIT Kanpur

March, 1999

To

my parents

Abstract

A numerical study of enhanced oil recovery from porous formations is presented in this work Resistance to oil movement arises from viscous as well as surface tension forces The goal of *enhanced oil recovery* techniques is to reduce these forces and improve the mobility of oil Thermal methods are frequently used to lower the oil viscosity, while surfactants are used to lower the surface tension The present study concerns modeling of the oil recovery by hot and cold water injection and the effect of surfactants on the enhancement of the oil recovery

Equations governing nonisothermal two-phase flow in a porous medium are obtained from the mass balance principle for the two phases, Darcy's law as applicable to an unsaturated porous region and the energy equation in terms of a local volume-averaged temperature These are supplemented by constitutive relations that connect the capillary pressure, relative permeability and the water saturation The governing equations are reduced to a coupled system of nonlinear partial differential equations in terms of oil and water pressures and temperature In the present study, pressure equations are solved using an implicit central difference scheme and saturation is determined from the difference between oil and water pressures The energy equation has been solved using an *operator splitting* (OS) algorithm

A *domain decomposition technique* has also been developed in the present work for solving the governing equations Domain decomposition is a useful method for solving problems over very large domains or regions having a complex geometry An attractive feature of this technique is the possibility of parallelizing the computer code suitable for computers with a parallel architecture In the present work, a completely parallel code has been developed for the oil recovery problem using the domain decomposition technique Results do show a great potential for this technique for simulating the field scale problems

The present study also concerns modeling of flow in a thick porous layer considered as a two-spot model to predict the actual flow behaviour that takes place in a five-spot model Results reveal the flow pattern of the field scale problems

Acknowledgements

It was a great opportunity for me to have worked under Prof. G. Biswas, who has provided me his unstinted support to carry out the work presented in this thesis I am indebted to him for his generous help through out Also I would like to express my sincere gratitude to Prof K Muralidhar for many fruitful discussions, invaluable suggestions, enormous help in cracking many tricky problems and constant encouragement

I thankfully acknowledge all the members of the F M & C F D Lab for their friendly behaviour and sincere cooperation

I am thankful to all of my friends especially Anjanda, Ghata, Nilanjan, Arunda, Pavitrada, Atul, Amit, Apurva and Shivesh for making my stay at IIT Kanpur enjoyable.

Above everything, constant encouragement, good wishes and blessings from my parents and other family members have been the source of inspiration throughout my thesis work

Partha Pratim Mukherjee

Contents

List of Figures

List of Tables

Nomenclature

Bi	Heat loss parameter
c	Specific heat capacity (J/kg-°C)
k_r	Relative permeability of phases
K	Absolute permeability of porous medium (Darcies)
K_h	Thermal conductivity of porous medium (W/m-°C)
p_{cow}	Capillary pressure of oil-water system (Pa)
$p_{o,w}$	Phase pressures of oil and water respectively (Pa)
$P_{1,2}$	Absolute pressures on injection and exit planes respectively (Pa)
S	Phase saturation
ppv	Percentage pore volume of oil recovery
$t, \triangle t$	Time and time step (s)
T	Temperature (°C)
T_f	Formation temperature (°C)
u	Darcy velocity vector (m/s)
x, y	Cartesian coordinates (m)
$\triangle x, \triangle y$	Grid size along x and y axes respectively (m)
X,Y	Domain dimensions along x and y axes respectively (m)

Greek Symbols

β	Expansivity ($°C^{-1}$)
ξ	Compressibility (Pa^{-1})
μ	Dynamic viscosity (Pa-s)
ρ	Density (kg/m^3)
$(\rho c)_R$	Heat capacity per volume of porous medium (J/m^3-°C)
ϵ	Porosity
ω	Interface convergence parameter

Superscript

n	Current time step

Subscript

i, j	Node indices along x and y axes respectively
o, w	Oil and water phases respectively
R	Rock formation

Chapter 1

Introduction

It has been recognised that the mankind is likely to face a critical shortage of petroleum all over the world in near future Under such a situation, exploring the possibility of enhancing the oil recovery from the existing reservoirs invariably assumes tremendous importance It is also well known that a large proportion of the existing oil reservoirs are still underrecovered The need for increasing the recovery of oil from such reservoirs calls for developing the enhanced oil recovery (EOR) techniques Particularly in our country, the availability of oil will play a vital role in the nation's competetiveness and industrial health over the next two decades Several natural resources of oil have been identified in the country, but all of these are being operated at the primary stage, with no enhancement technology Clearly there is a need for establishing the technology of EOR at the earliest And the objective of the present work is to consider the EOR techniques from numerical point of view and develop faster and more reliable numerical codes for reservoir simulation

The conventional methods of oil recovery, earlier to the advent of EOR techniques, can be categorised as the following

(1) Primary recovery In this case the in-situ pressure in the reservoir is often high enough to force the resident fluid out of the production wells without any pumping effort This accounts for 15%−20% of the total oil reserve

(2) Secondary recovery Here a fluid such as water is injected into some wells in the reservoir while petroleum is pushed through the production wells This serves the dual purpose of maintaining high reservoir pressure and of flooding the porous medium to physically displace some of the oil and push it towards the production wells But unfortunately,

waterflooding is still not extremely effective and significant amounts, upto 50% of hydrocarbon often remain in the reservoir Due to strong surface tension effects, a large amount of oil is trapped in small pores with narrow throats and is not washed out with routine waterflooding techniques

In order to recover more hydrocarbon, several enhanced oil recovery techniques involving complex chemical and thermal effects have been developed A brief overview of various EOR techniques is furnished here

(1) **Thermal recovery methods** (Boberg, 1988, Aziz, 1986) aim at reducing the oil viscosity by raising its temperature, thus improving the displacement efficiency of oil It involves injection of either hot water or steam into the reservoir via injection wells As the heated fluid comes into contact with the cooler oil, the temperature of oil is raised Consequently the oil viscosity is reduced and it is pushed rather easily through the porous formation Pushing the high temperature fluid down into the reservoir is a difficult engineering problem The hot injected fluid may lose heat while moving through the injection well and later to the host rock bounding the oil rich region Some energy is also consumed in the chemical reactions of hydrocarbons Apart from heat loss, one major problem is the gravity override This occurs when the hot fluid rises on to the top of the oil saturated sand layer and bypasses it If the flow rate is high, the interface between the resident petroleum and the invading displacing fluid can be unstable leading to the formation of long fingers These fingers grow in length towards the production wells, thus bypassing much of the oil Such factors cause a drastic reduction in oil production

(2) **Surfactant flooding** improves the oil displacement efficiency by reducing the interfacial tension between oil and water considerably Surfactants are surface active chemicals, a solution of which in water, injected at an appropriate pressure mobilizes the trapped oil to form a flowing oil bank by overcoming the capillary forces that are predominant in unsaturated porous regions

(3) **Polymer flooding** (Boberg, 1988, Shah *et al*, 1977) is used to increase the volume of the reservoir contacted by the displacing fluid Addition of a low concentration of polymer makes the floodwater more viscous, decreases its tendency to finger through and bypass oil, and leads to increased sweep of the reservoir. Polymer flooding, however, does not recover residual oil trapped in microscopic pores by capillary forces Therefore, it is very often viewed as an improved secondary recovery process rather than an EOR technique

(4) **In-situ combustion** technique is generally employed for reservoirs that are too deep to be mined and it calls for in-situ transformation of the hydrocarbons into states which can

be pumped to the surface via production wells. In this technique, the solid hydrocarbon is ignited in the ground and oxygen or air is pumped into the injection wells to maintain combustion The hot hydrocarbon gases are pumped to the surface via the production wells for use as low-grade hydrocarbon

Reservoir simulation is one of the most challenging problems in engineering (Ewing, 1983, Jim Douglas Jr , 1983). Owing to variety of contributing factors like the inherent complexity of the domain, complex nature of the constitutive relationships and instability of the oil-water interface the governing partial differential equations are highly non-linear and coupled Also analytical solutions are difficult to obtain. In the present work, we propose to perform the numerical simulation of the EOR technique using hot water injection. This aspect of the investigation is an extension of the earlier work (Pillai and Muralidhar, 1993) We also propose to investigate the effect of surfactants on oil recovery for a two-dimensional rectangular porous formation This part of the investigation is in continuation with the earlier work of Chatterjee and Muralidhar (1995) Also a numerical study has been done for a two-dimensional two-spot model, more precisely known as *quarter five-spot model* (Sorbie *et al* , 1995, Zhang *et al* , 1997) For the two-spot problem, we have studied the isothermal injection and also the effect of surfactants on oil recovery. For the numerical investigations mentioned above, a pressure based formulation (Ewing, 1983) has been used In the present study, pressure equations are solved using an implicit central difference scheme and saturation is determined from the difference between oil and water pressures The energy equation has been solved using an operator-splitting algorithm (Muralidhar *et al* , 1993) The presence of mass transfer phenomenon such as adsorption and desorption of surfactants from water to the solid matrix and vice versa is neglected in the present work

Computational time is an important issue while solving reservoir problems Because of high degree of non-linearity of the governing equations and large size of the reservoirs, reservoir simulation is computationally intensive. However, the current approach towards handling such complex problems is to improve the numerical algorithm on one hand and the computer performance is on the other With the advent of parallel computers there exists a great potential in increasing computer performance in terms of speed as well as memory In this context, domain decomposition techniques (Glowinski *et al* , 1983, Le Tallec, 1994) are very suitable for reservoir simulation Splitting the physical domain into sub-domains is the essential feature of the domain decomposition. The governing

equations are then solved independently in each sub-domain The individual solutions are subsequently assembled carefully to get a converged solution of the original problem on the complete physical domain Domain decomposition can rapidly make the simulation parallelizable since calculations in each sub-domain can be carried out independently on a processor They can also handle large problems on sequential machines more efficiently

A great amount of investigations on domain decomposition have appeared in the literature in the past few years Glowinski *et al.* (1983), have developed a number of efficient parallelizable domain decomposition algorithms in their pioneering work and these are in wide use Perng and Street, (1990) have applied domain decomposition technique to solve Navier-Stokes equations in complex domains which are otherwise difficult to solve without coordinate transformation Parallelizable domain decomposition codes applied to transient problems are however scant in literature Sequential domain decomposition codes applied to steady problems are available in plenty (Perng *et al*, 1990)

In the present work, we have developed a parallel code to solve the transient oil recovery problem for isothermal injection and the effect of surfactants (Muralidhar *et al*, 1996) has also been studied Uzawa's algorithm (Glowinski, 1983, Yagawa, 1991) has been used for interface treatment in conjunction with an implicit formulation The algorithm has the desired parallel and temporal properties Results are in excellent agreement with those due to the full domain simulation

The present work is organised along the following sequence.

- Mathematical modelling and formulation of the oil recovery problem.
- Overview of the numerical techniques developed and implemented for the simulation
- Results and discussions of the simulation of the EOR problem
- Conclusions and scope for the future work.

Chapter 2

Mathematical Model and Formulation of the Problem

In this chapter the mathematical formulation of the governing equations for two-phase flow through a porous media has been discussed The physical laws that govern multi-phase flow through the porous medium are

1 Conservation of mass of the individual phases,

2 Appropriate form of Darcy's law that includes capillary effects, and

3 Conservation of thermal energy

2.1 Assumptions

The following assumptions have been made in the present study

1 The fluid phases, namely oil and water flow simultaneously

2 Since the phase velocities are small, local thermal equilibrium between the fluid and solid phases is assumed

3 Gravity term is neglected in the momentum equation It is reasonable because the time frames are short and as a result the gravity override effect will not show up

4 The fluids, the solid matrix and the porous region are assumed to be incompressible and porosity is a constant

5 The fluids are immiscible, i e , there is no mass transfer between them

6 Relative permeabilities are taken as unique functions of saturation and viscosities as unique functions of temperature
7 Specific heats are assumed to be constant
8 There is no net mass source in the flow field
9 Viscous dissipation and mechanical work terms in the energy equation are neglected
10 Fluids, i e oil and water are assumed to exhibit Newtonian behaviour

2.2 Governing Equations

Equations governing transient two-phase flow through a homogeneous, isotropic porous medium are given as follows

Mass Balance

Accumulation rate + Efflux rate = Generation rate
i e

$$\frac{\partial}{\partial t}(\epsilon S_i \rho_i) + \nabla\,(\rho_i u_i) = 0 \qquad (i = \text{oil, water}) \tag{2 1}$$

(assuming no generation)

Darcy's Law

The momentum conservation equations for low Reynolds number, i e Re$\leq$1, assume the form of Darcy's laws which are given as follows

$$u_i = -\frac{K k_{ri}}{\mu_i} \nabla p_i \tag{2 2}$$

(neglecting the effect of gravity override)

Energy Equation

The rate at which thermal energy diffuses into a control volume is equal to the sum of the rate of accumulation and its efflux rate

$$\frac{\partial T}{\partial t} + UT_x + VT_y = \frac{K_h}{\sigma_T}\nabla^2 T \tag{2 3}$$

where

$$U = \frac{u_o\rho_o c_o + u_w\rho_w c_w}{\sigma_T}$$

$$V = \frac{v_o\rho_o c_o + v_w\rho_w c_w}{\sigma_T}$$

$$\sigma_T = \epsilon\{(1 - S_w)\rho_o c_o + S_w\rho_w c_w\} + (1 - \epsilon)(\rho c)_R$$

Constitutive relationships

$$\xi_i = \frac{1}{\rho_i}\left(\frac{\partial \rho_i}{\partial p_i}\right)_T \tag{2 4}$$

$$\beta_i = -\frac{1}{\rho_i}\left(\frac{\partial \rho_i}{\partial T}\right)_{p_i} \tag{2 5}$$

(from the definitions of the coefficient of compressibility and the coefficient of expansivity respectively)

$$p_{c_{ow}}(S_w) = p_o - p_w \tag{2 6}$$

($p_{c_{ow}}$ is capillary pressure and a unique function of S_w)

$$S_o + S_w = 1 \tag{2 7}$$

(Here we assume that the pore volume not occupied by oil, is occupied by water and no gas phase is present)

$$k_{ri} = k_{ri}(S_w) \tag{2 8}$$

(i e relative permeability of a phase is a unique function of saturation)

Equations 2 1 and 2 2 can be combined to generate two equations for oil and water respectively, using the constitutive relationships These equations are as follows

$$-S_o\beta_o\frac{\partial T}{\partial t} + S_o\xi_o\frac{\partial p_w}{\partial t} - \frac{dS_w}{dp_{c_{ow}}}\left[\frac{\partial p_o}{\partial t} - \frac{\partial p_w}{\partial t}\right] = \frac{1}{\rho_o}\nabla\left[\frac{Kk_{ro}\rho_o}{\mu_o\epsilon}\right]\nabla p_o \tag{2 9}$$

$$-S_w\beta_w\frac{\partial T}{\partial t} + S_w\xi_w\frac{\partial p_w}{\partial t} + \frac{dS_w}{dp_{c_{ow}}}\left[\frac{\partial p_o}{\partial t} - \frac{\partial p_w}{\partial t}\right] = \frac{1}{\rho_w}\nabla\left[\frac{Kk_{rw}\rho_w}{\mu_w\epsilon}\right]\nabla p_w \tag{2 10}$$

It is extremely important to justify the use of the pressure formulation at this stage Oil recovery problem can also be formulated in terms of water saturation This means that the three dependent variables which will appear in the coupled system of non-linear partial differential equations will be in this case oil pressure, water saturation and temperature instead of oil and water pressures and temperature However this approach can lead to difficulties in numerical computation since the oil-water interface can be quite sharp In contrast to this, the pressure field must be continuous everywhere This results in appreciable improvement in the accuracy of the numerical simulation

2.3 Physical Description

The problem of interest considers flow through a thin porous layer and a thick porous layer

The physical domain for the flow through a thin porous layer is shown in Figure 2 1 The flow is two dimensional and the rectangular domain has a nominal size of 10 m × 1 2 m. Essentially we are studying the water piston effect in a rectangular domain packed with sand and guarded with impermeable but thermally conductive rocks above and below the porous region (called overhang and underhang respectively)

The physical domain for the flow through a thick porous layer is shown in Figure 2.2 The geometric model is the much talked about five-spot model (Figure 2 2 (a)) The flow is essentially two-dimensional and the square domain (the plan view of the thick porous layer) has a nominal size of 6 m × 6 m We have, however, studied the flow for the quarter five-spot model (hereafter mentioned as two-spot model; Figure 2 2 (b)) We aim at simulating the flow for a set of three simplified versions (Figure 2 2 (c), (d) and (e)) of the original two-spot model Barring the regions for injection and production wells, the sand packed domain is guarded with impermeable rocks

Initially the porous medium is impregnated with oil to a given saturation It has some initial temperature, called the formation temperature and is at rest One of the assumptions in this study is that the pore volume not containing oil has water. At equi-

librium, the oil and water pressures in the porous layer can be uniquely determined from their saturation Oil recovery is initiated by pushing water at a given higher pressure and a given temperature We observe the movement of saturation and temperature profiles in the porous region

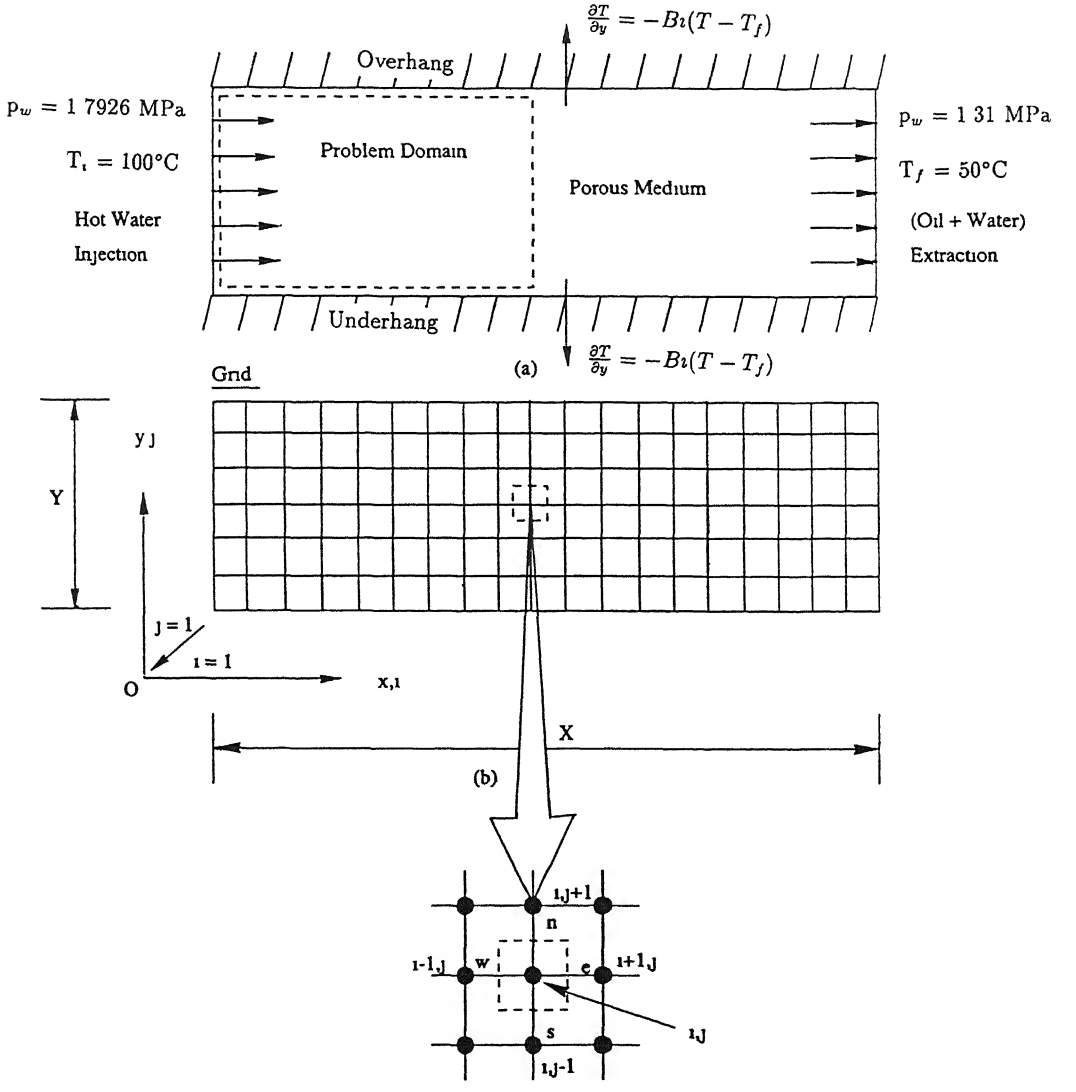

Figure 2 1 Description of the Oil Recovery Problem from Thin Porous Formation

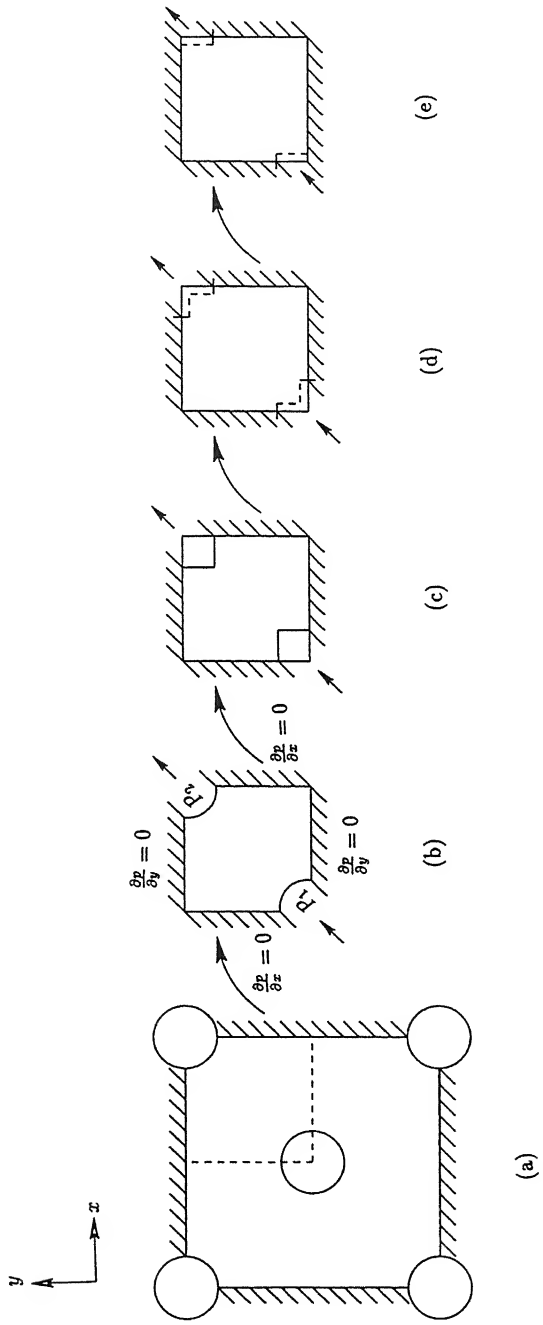

Figure 2 2. Description of the Oil Recovery Problem from Thick Porous Formation

We have addressed to two variants of the main physical phenomena in this study as furnished below

(1) Isothermal Problem In this case the high pressure water is injected at a temperature same as that of the formation temperature The effect of surfactants is also considered for this case We have accomplished this study for both the thin porous formation and the thick porous formation Essentially we need not solve the energy equation herein

(2) Non-isothermal Problem The problem of interest involves transportation of thermal energy into the flow domain through hot water that is injected at a higher pressure Naturally the temperature distribution is important in this case and the energy equation is solved along with the pressure equations However, we have undertaken this study only for the thin porous formation

2.4 Initial and Boundary Conditions

The pressure equations (equations 2 9 and 2.10) are solved for both the rectangular and the square flow domains subject to a quiescent initial condition, impermeable confining walls and specified oil and water pressures at the inflow and outflow sections At the injection zone of the domain, the water is at a pressure of 1 7926 MPa and at a temperature of 100°C Saturation of water is 0 86 here It is not unity because of the presence of some residual oil which cannot be flushed out It is by far the maximum water saturation possible anywhere in the domain. At the production zone of the domain, water pressure, temperature and saturation are maintained at 1.31 MPa, 50°C and 0 2 respectively Obviously the injection water temperature is 100°C only for the non-isothermal injection, otherwise the temperature is same as that of the production zone

Initially, the porous region is maintained at a uniform water pressure and temperature of 1 31 MPa and 50°C respectively and the oil saturation is of 0.8 Oil pressure is obtained by adding water pressure to the capillary pressure, the latter being a unique function of the water saturation.

The impermebility condition at the bounding surfaces calls for the Darcy velocity components becoming zero, which give rise to the boundary conditions as,

$$\frac{\partial p_i}{\partial x} = \frac{\partial p_i}{\partial y} = 0$$

Boundary condition related to heat loss to overhang and underhang correponding to the thin porous layer flow domain is given by

$$\frac{\partial T}{\partial y} + Bi(T - T_f) = 0 \qquad \text{at y} = 0, \text{ Y}$$

The model presented in this work, predicts the movement of the water front from the injection zone into the oil-rich porous region This increase in water saturation is a measure of the amount of oil displaced Oil displacement is measured in terms of the percentage pore volume (*ppv*) It is defined as,

$$ppv = 100 \times \frac{\text{total volume of oil produced}}{\text{total pore volume}}$$

The use of Dirichlet boundary condition at the outflow section is justified only if the location of this section is far away from the injection region In the present study, oil recovery is computed over half a distance of the domain size For a five hour simulation, considered here, numerical experiments show that oil recovery is insensitive to the location of the outflow section

The data for the parametric values and constitutive relationships used in the present study have been mostly adapted from Boberg (1988) and are given in Appendix A

Chapter 3

Numerical Scheme

In this chapter we shall discuss, in detail, the numerical techniques used for solving the governing differential equations enumerated earlier Also the implementation of the domain decomposition technique will be taken up in our discussion

3.1 Discretization of Pressure Equations

The oil and water pressure equations 2 9 and 2 10 are discretized using a control volume finite difference scheme for both the flow domains (Figure 2 1 (a) and Figure 2 2 (b)). The scheme is fully implicit in time This implies that all spatial derivatives are evaluated at the new time step The time derivatives of pressure are discretized using the forward difference technique and those of temperature using the backward difference technique However the backward differencing in time of the temperature term is justified because the effect of temperature on the pressure distribution is brought about through the fluid properties The fluid properties do not change as rapidly with time as the primary variables like phase pressures and saturation The final form of the discretized pressure equations are

$$[A_o p_{o_{i+1,j}} + B_o p_{o_{i,j}} + C_o p_{w_{i,j}} + D_o p_{o_{i-1,j}} + E_o p_{o_{i,j+1}} + F_o p_{o_{i,j-1}}]^{n+1} = G_o \qquad (3.1)$$

$$[A_w p_{w_{i+1,j}} + B_w p_{w_{i,j}} + C_w p_{o_{i,j}} + D_w p_{w_{i-1,j}} + E_w p_{w_{i,j+1}} + F_w p_{w_{i,j-1}}]^{n+1} = G_w \qquad (3.2)$$

where,

$$A_o = -\left\{\frac{\theta_e}{\rho_{o_{i,j}}(\triangle x)^2}\right\}^{n+1}$$

$$B_o = \frac{S_{o_{i,j}}^{n+1}\xi_o - \left(\frac{dS_w}{dp_{cow}}\right)_{i,j}^{n+1}}{\triangle t} + \frac{1}{\rho_{o_{i,j}}^{n+1}}\left\{\frac{\theta_e+\theta_w}{(\triangle x)^2} + \frac{\theta_n+\theta_s}{(\triangle y)^2}\right\}^{n+1}$$

$$C_o = \left(\frac{dS_w}{dp_{cow}}\right)_{i,j}^{n+1}\frac{1}{\triangle t}$$

$$D_o = -\left\{\frac{\theta_w}{\rho_{o_{i,j}}(\triangle x)^2}\right\}^{n+1}$$

$$E_o = -\left\{\frac{\theta_n}{\rho_{o_{i,j}}(\triangle y)^2}\right\}^{n+1}$$

$$F_o = -\left\{\frac{\theta_s}{\rho_{o_{i,j}}(\triangle y)^2}\right\}^{n+1}$$

$$G_o = \left\{\frac{S_{o_{i,j}}\xi_o - \left(\frac{dS_w}{dp_{cow}}\right)_{i,j}}{\triangle t}p_{o_{i,j}}\right\}^n + \left\{\frac{1}{\triangle t}\left(\frac{dS_w}{dp_{cow}}\right)_{i,j}p_{w_{i,j}}\right\}^n + S_{o_{i,j}}^n\beta_o\frac{T_{i,j}^n - T_{i,j}^{n-1}}{\triangle t}$$

and

$$A_w = -\left\{\frac{\gamma_e}{\rho_{w_{i,j}}(\triangle x)^2}\right\}^{n+1}$$

$$B_w = \frac{S_{w_{i,j}}^{n+1}\xi_w - \left(\frac{dS_w}{dp_{cow}}\right)_{i,j}^{n+1}}{\triangle t} + \frac{1}{\rho_{w_{i,j}}^{n+1}}\left\{\frac{\gamma_e+\gamma_w}{(\triangle x)^2} + \frac{\gamma_n+\gamma_s}{(\triangle y)^2}\right\}^{n+1}$$

$$C_w = \left(\frac{dS_w}{dp_{cow}}\right)_{i,j}^{n+1}\frac{1}{\triangle t}$$

$$D_w = -\left\{\frac{\gamma_w}{\rho_{w_{i,j}}(\triangle x)^2}\right\}^{n+1}$$

$$E_w = -\left\{\frac{\gamma_n}{\rho_{w_{i,j}}(\triangle y)^2}\right\}^{n+1}$$

$$F_w = -\left\{\frac{\gamma_s}{\rho_{w_{i,j}}(\triangle y)^2}\right\}^{n+1}$$

$$G_w = \left\{\frac{S_{w_{i,j}}\xi_w - \left(\frac{dS_w}{dp_{cow}}\right)_{i,j} p_{w_{i,j}}}{\triangle t}\right\}^n + \left\{\frac{1}{\triangle t}\left(\frac{dS_w}{dp_{cow}}\right)_{i,j} p_{o_{i,j}}\right\}^n + S^n_{w_{i,j}}\beta_w \frac{T^n_{i,j} - T^{n-1}_{i,j}}{\triangle t}$$

where

$$\theta = \frac{Kk_{ro}\rho_o}{\epsilon\mu_o}$$

$$\gamma = \frac{Kk_{rw}\rho_w}{\epsilon\mu_w}$$

Here $(\theta_e, \theta_w, \theta_n, \theta_s)$ and $(\gamma_e, \gamma_w, \gamma_n, \gamma_s)$ are values corresponding to the points lying towards the east, west, north and south of the node i, j (as shown in the Figure 2 1 (b)) and are evaluated as the harmonic averages of the values at nodes that lie on either side

The oil pressure equation 3 1 and the water pressure equation 3 2 are written for every node on the grid mesh to obtain a set of $2 \times n \times m$ simultaneous eqations These equations can be written in a matrix form The matrix thus obtained is banded The matrix structure is shown in Figure 3 1 It has been solved by using a specialized sparse matrix solver based on Gaussian elimination (Duff, 1980) and also by preconditioned conjugate gradient method (PCG; Muralidhar and Sundararajan, 1995)

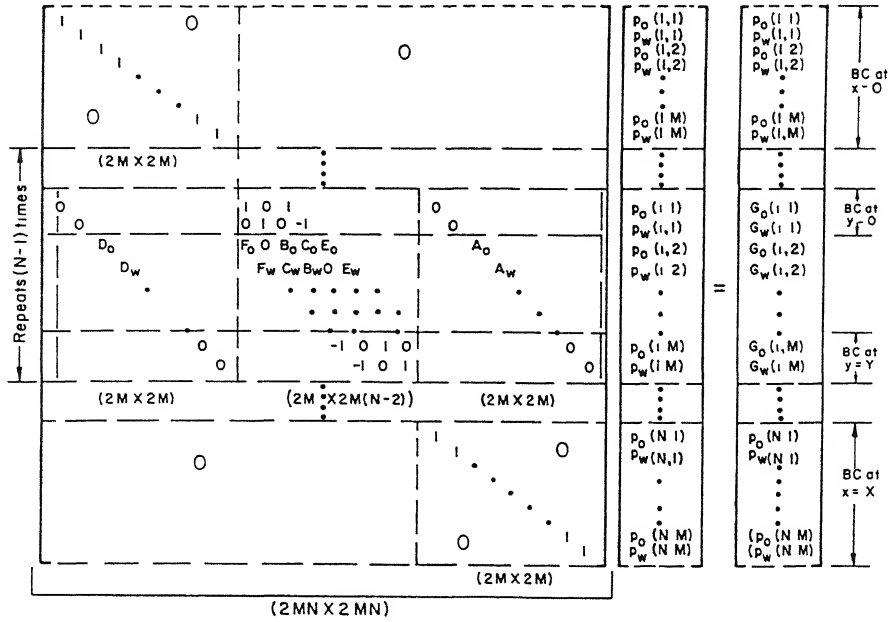

Figure 3 1 Matrix Structure in Pressure Calculation

3.2 Solution of the Energy Equation

The energy equation is solved by using the *operator splitting algorithm* The energy equation,

$$\frac{\partial T}{\partial t} + U\frac{\partial T}{\partial x} + V\frac{\partial T}{\partial y} = \left(\frac{K_h}{\sigma_T}\right)\nabla^2 T \tag{3 3}$$

is split into the following steps

Predictor:

$$\frac{\partial T}{\partial t} + U\frac{\partial T}{\partial x} + V\frac{\partial T}{\partial y} = 0 \tag{3 4}$$

Corrector:

$$\frac{\partial T}{\partial t} = \left(\frac{K_h}{\sigma_T}\right)\nabla^2 T \tag{3 5}$$

3.2.1 Solution of the Predictor Step Using Streamlines

We choose a curvilinear coordinate system (ξ, η) locally at each node such that $\nabla\xi$ is aligned with the net fluid composite velocity at that node, i e ξ is streamline passing

through the node (Figure 3 2 (a)) Then

$$UT_x + VT_y = U'T_\xi \tag{3 6}$$

where, $U' = \sqrt{U^2 + V^2}$

Hence the predictor equation becomes

$$T_t + U'T_\xi = 0 \tag{3 7}$$

The solution of this equation is $T(U't - \xi) = \text{Constant}$

The solution of the Predictor step requires that the temperature at Q at the n^{th} timestep be transferred to the point P at $(n+1)^{th}$ time step (Figure 3 2 (b)), i e

$$T_P^{n+1}(U'(t + \triangle t) - \xi) = T_Q^n(U't - (\xi - \triangle\xi))$$

where, $\triangle\xi = U'^n \triangle t$

The temperature T_Q is obtained through interpolation

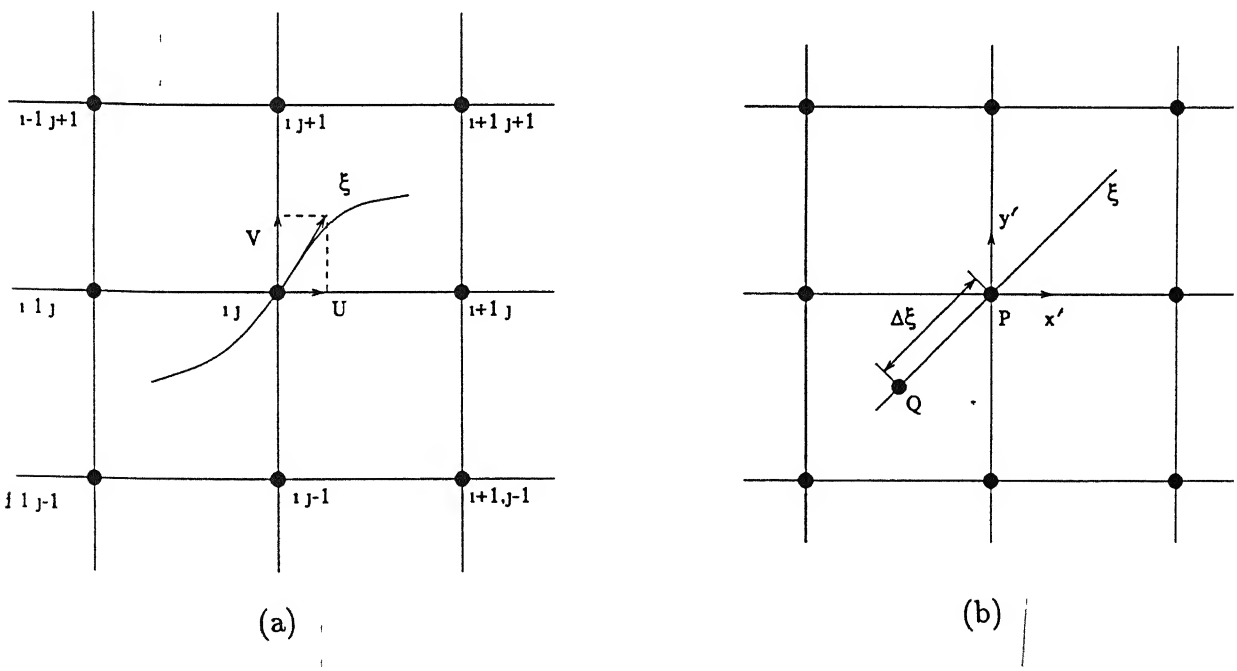

Figure 3 2 Solution of Predictor of the Energy Equation.

3.2.2 Solution of the Corrector Step Using ADI

The corrector step consists of the two-dimensional unsteady state heat conduction equation It is solved using the *Alternating Direction Implicit* (ADI) technique In ADI, we first compute row by row intermediate temperatures while sweeping along the j-axis Then by sweeping along the i-axis final temperatures for the time step are calculated in the column by column fashion The time step for each sweep is $(\triangle t)_{adi} = \triangle t/2$ The discretization is given as

Sweeping along j-axis:

$$T_i^{n+\frac{1}{2}} - T_{i,j}^n = \frac{(\triangle t)_{adi}}{Pe} \left\{ \left[\frac{T_{i+1,j} + T_{i-1,j} - 2T_{i,j}}{(\triangle x)^2} \right]^{n+\frac{1}{2}} + \left[\frac{T_{i,j+1} + T_{i,j-1} - 2Ti,j}{(\triangle y)^2} \right]^n \right\} \quad (3\,8)$$

or

$$\{AT_{i-1,j} + B_{left}Ti,j + CT_{i+1,j}\}^{n+\frac{1}{2}} = \{B_{right}T_{i,j} + DT_{i,j+1} + ET_{i,j-1}\}^n \quad (3\,9)$$

where

$$A = C = \frac{(\triangle t)_{adi}}{Pe(\triangle x)^2}, \quad B_{left} = 1 + \frac{2(\triangle t)_{adi}}{Pe(\triangle x)^2},$$

$$D = E = \frac{(\triangle t)_{adi}}{Pe(\triangle y)^2}, \quad B_{right} = 1 - \frac{2(\triangle t)_{adi}}{Pe(\triangle y)^2}$$

$$\text{and,} \quad \text{Pe} = \text{Equivalent Peclet Number} = \frac{\sigma_{\text{T}}}{\text{K}_{\text{h}}}$$

Sweeping along i-axis:

$$T_{i,j}^{n+1} - T_{i,j}^{n+\frac{1}{2}} = \frac{(\triangle t)_{adi}}{Pe} \left[\left\{ \frac{T_{i+1,j} + T_{i-1,j} - 2T_{i,j}}{(\triangle x)^2} \right\}^{n+\frac{1}{2}} + \left\{ \frac{T_{i,j+1} + T_{i,j-1} - 2T_{i,j}}{Pe(\triangle y)^2} \right\}^{n+1} \right] \quad (3\,10)$$

or

$$\{AT_{i,j-1} + B_{left}T_{i,j} + CT_{i,j+1}\}^{n+1} = \{B_{right}T_{i,j} + DT_{i+1,j} + ET_{i-1,j}\}^{n+\frac{1}{2}} \qquad (3\ 11)$$

where

$$A = C = -\frac{(\triangle t)_{adi}}{Pe(\triangle y)^2}, \quad B_{left} = 1 + \frac{2(\triangle t)_{adi}}{Pe(\triangle y)^2},$$

$$D = E = \frac{(\triangle t)_{adi}}{Pe(\triangle x)^2}, \quad B_{right} = 1 - \frac{2(\triangle t)_{adi}}{Pe(\triangle x)^2}$$

The equations are written for every node in the row or column and the set of simultaneous equations thus obtained yields a tridiagonal matrix, which can be inverted using TDMA as a matrix solver

3.3 Algorithm

The system of equations governing the distribution of oil and water pressures and temperature are non-linear and mutually coupled They are solved simultaneously and by iteration

The algorithm, in brief, is as folows

(1) The initial distributions of p_o, p_w, T and S_w at $t = 0$ are prescribed

(2) The coefficients ($A_o - G_o$ and $A_w - G_w$) of the prssure equations are computed using the values of p_o, p_w, T and S_w at the current time step and iteration level

(3) The system of pressure equations is solved to obtain the new values of p_o and p_w at the nodes formed by the grid

(4) S_w, ρ_o and ρ_w are updated via the constitutive relations using the new pressure values

(5) Darcy velocities are calculated using the latest values of p_o, p_w, S_w, ρ_o and ρ_w

(6) Using S_w, ρ_o, ρ_w and the Darcy velocities, the coefficients of the energy equation are computed and the equation is solved using the OS algorithm which yields new temperature distribution

(7) ρ_o and ρ_w are updated once again using the new value of temperature The fluid viscosities are also updated at this stage

(8) Steps (2) – (7) are repeated until convergence of p_o, p_w and T is achieved
(9) Fresh computation is initiated for the next time step starting from step (2)

The above algorithm is used when the energy equation is involved, but for the isothermal injection, steps (5), (6) and (7) invariably become redundant

3.4 Operator Splitting Algorithm

3.4.1 Introduction

The operator splitting algorithm (OS) is a special case of splitting methods or fractional step methods which reduces the solution of a complicated problem to a successive solution of simpler problems Various forms of splitting methos, such as, geometric splitting, physical splitting and analytical splitting are available The OS algorithm used for the present investigation, belongs to the analytical splitting family This algorithm properly identifies the mixed mathematical character of the governing differntial equation and solves each homogeneous component of the equation as accurately as possible Hence the OS algorithm solves the governing equation true to its character

3.4.2 Model Example

Let us consider a typical convection-diffusion problem (Muralidhar *et al*, 1993) arising in heat transfer problems of the form,

$$\frac{\partial T}{\partial t} + (\tilde{u}\ \tilde{\nabla})T = \alpha \nabla^2 T \tag{3 12}$$

The mathematical character of the equation is elliptic if t$\rightarrow \infty$, parabolic if $\tilde{u}$ is small and hyperbolic if $\tilde{u}$ is large in magnitude In all other cases, the equation is said to be mixed in character These special cases are summarised below

$$\text{Steady state} \quad (t \rightarrow \infty) \quad (\tilde{u}\ \tilde{\nabla})T = \alpha \nabla^2 T \quad \text{(elliptic)} \tag{3 13}$$

$$\text{Conduction limit} \quad (|\ \tilde{u}\ | \rightarrow 0) \quad T_t = \alpha \nabla^2 T \quad \text{(parabolic)} \tag{3 14}$$

$$\text{Convection limit} \quad (|\ \tilde{u}\ | \rightarrow \infty) \quad T_t + \tilde{u}\ \tilde{\nabla} T = 0 \quad \text{(hyperbolic)} \tag{3 15}$$

The OS algorithm handles this problem along the following line
(1) At any time level t, equation (3 15) is solved over a time step Δt This is the predictor step
(2) The equation (3 14) is then solved over the same time interval Δt and this is considered as the corrector step

At high values of velocity, the correction required is quite small and and at low velocities the predictor step acting alone is inadequate However, the two steps combined will furnish the complete solution of the equation (3 12) irrespective of the magnitude of $\tilde{u}$

3.4.3 Remarks

The salient features of the OS algorithm are depicted below

1. The scheme is completely free of upwinding and hence devoid of false diffusion errors that usually occur at high Peclet numbers

2 The only error arising in the OS algorithm is due to time discretization and it is of the order Δt When either of the predictor or corrector equation is solved numerically on a grid mesh of size Δx, then additional truncation errors ($\sim \quad \Delta x^n, \; n \geq 1$) creep in Hence the overall error is,

$$e \sim \bigcirc (\Delta x^n, \; \Delta t), \quad n \geq 1$$

where, n depends on the scheme used to solve the diffusive corrector step In our case for the corrector step, we have used a second order finite difference scheme and naturally the discretization error will be,

$$e \sim \bigcirc (\Delta x^2, \; \Delta t)$$

3. The main source of error in solving heat transfer problem lies in approximating the hyperbolic terms $(\tilde{u}.\tilde{\nabla}T)$ In the OS algorithm, these terms are treated analytically and solved as accurately as possible. In the oil recovery problem it has been solved on a local grid (Section 3 2 1)

4 On non-dimensionalisation, the heat transfer equation becomes

$$\frac{\partial T}{\partial t} + (\tilde{u}\ \tilde{\nabla})T = \frac{1}{Pe}\nabla^2 T$$

where, Pe is the Peclet number and is a measure of relative importance of convective transport with respect to diffusive transport It has been found from numerical experimentation that most of the existing algorithms fail or become inaccurate when Pe is high The OS algorithm has been found to be uniformly valid over any range of Pe As the Pe is raised, a discontinuity in the initial condition will propagate through the flow domain unchanged and is called a front Also fronts can be formed in non-linear problems at low or moderate Peclet numbers The oil recovery problem considered here is one such problem

5 The OS algorithm is conditionally stable since it involves explicit time marching and is limited by the Courant-Friedrichs-Lewy (CFL) stability criterion

3.5 Preconditioned Conjugate Gradient Method

3.5.1 Introduction

The Conjugate Gradient method can be used for inverting symmetric positive definite matrices It combines features of both iterative and direct solvers It converges faster than the Gauss-Siedel iteration for a given initial guess, but needs more arithmetic operations per iteration This method minimises an error functional along mutually conjugate directions in each iteration Hence for a functional defined in N dimensions, it converges theoretically in N iterations For a matrix with a small spectral condition number, convergence is attained in just a few iterations, much less than N This method is particularly suitable for sparse matrices The CG algorithm stated for a matrix equation $AX = b$ is as follows

1 Assume $X = X^0$ (initial guess)

2. Compute residue

$$r^k = b - Ax^k$$

3 Set the direction vector

$$P^k = r^k$$

4 Compute steepest descent parameter, α

$$\alpha = \frac{(r^k, r^k)}{(P^k, AP^k)}$$

5 Update the values of x and r

$$x^{k+1} = x^k + \alpha p^k$$

$$r^{k+1} = r^k - \alpha A p^k$$

6 Compute β

$$\beta = \frac{(r^{k+1}, r^{k+1})}{(r^k, r^k)}$$

7 Update the direction vector

$$P^{k+1} = r^{k+1} + \beta P^k$$

8 Check for convergence in x

9 Repeat steps 4 to 8 till convergence

The above algorithm cannot be applied directly to a matrix which is not positive definite and symmetric Preconditioning is required for such matrices The rate of convergence depends upon the the spectral condition number of the matrix The Spectral condition number is defined as the ratio of maximum eigenvalue to the minimum eigenvalue of the matrix Closer it is to unity faster would be the convergence This requires the eigenvalues to cluster around a certain number. The aim of preconditioning is to improve the spectral condition number and move it towards unity. It involves the choice of a suitable positive definite matrix M so that $AX = b$ may be replaced by $M^{-1}AX = M^{-1}b$, where $M^{-1}A$ should have a large number of its eigenvalues closely grouped

Three preconditioning strategies namely, (a) preconditioning I (symmetric matrices), (b) preconditioning II (asymmetric matrices) and (c) diagonal scaling have been described here

3.5.2 Preconditioning I (symmetric matrices)

The equation $AX = b$ is written as $(LL^T)^{-1}AX = (LL^T)^{-1}b$ where L is the lower triangular matrix, which may be computed efficiently by Cholesky decomposition The Cholesky method is suitable only for symmetric matrices since an asymmetric matrix can not be factored as LL^T If an approximate L matrix is used, Incomplete Cholesky Conjugate Gradient method (ICCG) is generated The complete algorithm is as follows

1 Assume $X = X^0$ (Initial guess)

2 Compute residue

$$r^k = b - AX^0$$

3 Set the direction vector

$$P^k = \left(L^T L\right)^{-1} A^T \left(LL^T\right)^{-1} r^k$$

4 Compute steepest descent parameter,α

$$\alpha = \frac{(r^k, (LL^T)^{-1} r^k)}{(P^k, (L^T L) P^k)}$$

5 Update the values of x and r

$$r^{k+1} = r^k - \alpha A P^k$$

$$X^{k+1} = X^k + \alpha P^k$$

6 Compute β

$$\beta = \frac{(r^{k+1}, (LL^T)^{-1} r^{k+1})}{(r^k, (LL^T)^{-1} r^k)}$$

7 Update the direction vector

$$P^{k+1} = [(L^T L)^{-1} A^T (LL^T)]^{-1} r^{k+1} + \beta P^k$$

8 Set $k = k + 1$, check for convergence in X.

9 Repeat steps 4 to 8 till convergence

3.5.3 Preconditioning II (asymmetric matrices)

For asymmetric non singular matrices the cholesky decomposition is replaced by the LU decomposition where we take unit diagonal elements in the upper triangular matrix U If L and U used have the same structure as A then the LU Decomposition Conjugate Gradient Algorithm (ILUCG) is generated Complete algorithm is as follows

1 Assume $X = X^0$ (Initial guess)

2 Compute residue

$$r^k = b - AX^0$$

3 Set the direction vector

$$P^k = \left(U^T U\right)^{-1} A^T \left(LL^T\right)^{-1} r^k$$

4 Compute steepest descent parameter,α

$$\alpha = \frac{(r^k, (LL^T)^{-1} r^k)}{(P^k, (U^T U) P^k)}$$

5 Update the values of x and r

$$r^{k+1} = r^k - \alpha A P^k$$

$$X^{k+1} = X^k + \alpha P^k$$

6 Compute β

$$\beta = \frac{(r^{k+1}, (LL^T)^{-1} r^{k+1})}{(r^k, (LL^T)^{-1} r^k)}$$

7 Update the direction vector

$$P^{k+1} = [(U^T U)^{-1} A^T (LL^T)]^{-1} r^{k+1} + \beta P^k$$

8 Set $k = k + 1$, check for convergence in X.

9 Repeat steps 4 to 8 till convergence

3.5.4 Diagonal Scaling

This strategy involves the scaling of matrix A so that the diagonal entries are strengthened with respect to the other elements within the matrix.

$$D^{-1/2} A D^{-1/2} D^{1/2} X = D^{-1/2} b$$

$$AX = b$$

$$A = D^{1/2} A D^{1/2}$$

$$X = D^{1/2} X$$

$$b = D^{-1/2} b$$

where D is the matrix containing only the diagonal entris of A

We have applied PCG for solving the banded matrix arising out of the pressure equations as a substitute to the specialized sparse matrix inverter based on Gaussian elimination and the results are seen to be matching nicely

3.6 Introduction to Domain Decomposition for Solving PDEs

3.6.1 Opening Remarks

Practical engineering problems inevitably require intensive computations because of the large size of physical domains and their complex geometries In many cases the computations cannot be implemented on existing computers owing to limitations of memory The current approach towards handling complex problems is to improve the numerical algorithm on one hand and the computer performance on the other With the advent of parallel computers there exists a great potential for increasing computer performance in terms of speed as well as memory However, parallel computers require parallel algorithms to make use of the distributed nature of the processor architecture *Domain decomposition techniques* are the simplest of parallel algorithms that can convert a sequential algorithm to one suitable for parallel computing Besides the ability to parallelize, other specific advantages of domain decomposition are

1 It can generate smaller matrices that require less memory and are rapidly invertible when iterative techniques are used

2 A complex assemblage of components of a system can be systematically analysed

3. Complex phenomena can be localized by assigning separate subdomains to them

3.6.2 Domain Decomposition and Uzawa's Algorithm

The basic approach of domain decomposition is that a large domain is divided into many subdomains that are linked at the interfaces The governing equations are then solved independently in each subdomain with assumed interface conditions The efficiency and accuracy of domain decomposition lies in its interface treatment Among the various interface treatments available for domain decomposition, *Uzawa's algorithm* has been shown to be robust and parallelizable It is analytically well-behaved and shows monotone convergence properties

Uzawa's algorithm for an elliptic problem is presented below. Consider the linear governing differential equation

$$\Delta u = f \quad \text{in } \Omega \tag{3 16}$$

$$\text{and} \quad u = g \quad \text{on } \partial\Omega$$

Here f and g are known functions, Ω is the physical region, $\partial\Omega$ is its boundary (Figure 3 3) and Δ is the Laplacian Operator Figure 3 3 also shows a decomposition of Ω into two

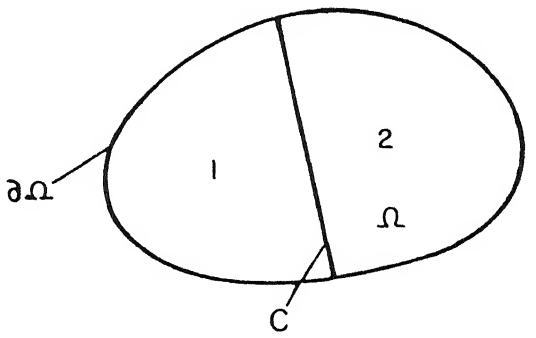

Figure 3 3 Physical Region and its Division into Two Subdomains

subdomains, 1 and 2, with C as their interface For a globally converged solution both u and its normal derivative are required to be continuous on C A start is made with a guess for

the derivatives, $\left.\frac{\partial u}{\partial n_1}\right|$ and $\left.\frac{\partial u}{\partial n_2}\right|$ $(= \lambda)$, where n_1 and n_2 are the normals at C extended into subdomains 1 and 2 respectively Using $\lambda^{(1)}$ as the boundary condition on C the governing differential equation is solved in regions 1 and 2 Let these solutions respectively be ${u_1}^{(1)}$ and ${u_2}^{(1)}$ Let ${y_1}^{(1)}$ and ${y_2}^{(1)}$ be the values of ${u_1}^{(1)}$ and ${u_2}^{(1)}$ respectively on C Then $\lambda^{(1)}$ is updated as

$$\lambda^{(2)} = \lambda^{(1)} + \frac{\omega\left({y_2}^{(1)} - {y_1}^{(1)}\right)}{L} \tag{3 17}$$

Here ω is an adjustable constant that lies between 0 and 1 and L is a suitable length scale It is taken to be the unity in the present work Using $\lambda^{(2)}$ as the next guess, the entire process is repeated After I iterations, Uzawa's algorithm for updating the interface flux is

$$\lambda^{(I+1)} = \lambda^{(I)} + \frac{\omega\left({y_2}^{(I)} - {y_1}^{(I)}\right)}{L} \tag{3 18}$$

Interface convergence is judged by the criterion

$$\left|\lambda^{(I+1)} - \lambda^{(I)}\right| \leq \delta$$

where δ is the specified upper bound The iterations of the algorithm given above converge when the computed function $u^{(I)}(x)$ matches the steady state solution of Equation (3 16)

For transient problems, the approach adopted has been to apply the same algorithm between the successive time steps Each subproblem in the subdomain is solved by an implicit finite differnce scheme The choice of the implicit scheme guarantees the stability of the time-marching procedure and rate of convergence is dictated by the magnitude of the interface parameter ρ alone When the gradient of the dependent variable converges, the variable at the interface becomes continuous, and this is implied by equation (3.18) Hence the algorithm ensures continuity of u as well as its normal derivative at the interface. The only difficulty with Uzawa's algorithm is in the choice of interface parameter ρ and must come from numerical experiments.

Equation (3.18) shows that domain decomposition introduces interface iterations, even in linear problems Hence the possibility of an increase in CPU time must be con-

sidered, especially under transient conditions But it has been seen that actually the CPU time decreases The reason for obtaining this result is the following When matrix inversion is accomplished using iterative methods, for example the Gauss-Siedel method, the convergence rate varies as $N^{-\alpha}$, where N is the matrix size and α is some positive constant Hence convergence is significantly delayed for large values of N Application of domain decomposition cuts the matrix size by a factor, ≥ 2, depending on the number of subdomains used Hence each subdomain calculation is accelerated, providing an overall computing time advantage

3.6.3 Domain Decomposition for Non-linear Problems

In case of a non-linear problem, the interface treatment must be modified Let us take up an example to illustrate this point Consider the linear heat conduction problem in the same domain as in Figure

$$K\nabla^2 T = \rho c_p \frac{\partial T}{\partial t} \tag{3.19}$$

where K, ρ and c_p are constants In Equation (3 19) the boundary conditions to be matched at the interfaces of the subdomains would be the temperature and the temperature derivative, $\frac{\partial T}{\partial n}$ This is both physically and mathematically conceivable Consider the non-linear problem,

$$\nabla\ K\nabla T = \rho c_p \frac{\partial T}{\partial t} \tag{3 20}$$

where K is taken as a function of temperature The physically conceivable Neumann boundary condition to be matched at the interface would be not the derivatives of T but the fluxes at the interface, $-K(T)\frac{\partial T}{\partial n}$ In the case of a linear problem, this boils down to the temperature derivatives alone, since K is not a function of temperature Thus for the non-linear problem, global convergence requires

$$-K\left(T_1{}^I\right)\left.\frac{\partial T_1{}^I}{\partial n_1}\right|_C = K\left(T_2{}^I\right)\left.\frac{\partial T_2{}^I}{\partial n_2}\right|_C \tag{3 21}$$

It should be noted that during iterations $T_1{}^I \neq T_2{}^I$ Also in inhomogeneous media with sharp change in thermal conductivity at the interface, heat fluxes rather than the temperature gradients should be matched

3.6.4 Simulation of EOR Using Domain Decomposition

Let us now consider the simulation of the oil recovery problem for the thin porous formation flow domain (Figure 2 1 (a)) using domain decomposition The initial and boundary conditions are identical to those considered in Section 2 4 Uzawa's algorithm is used for interface treatment The computer code is thus suitable for parallelization The same implicit pressure based formulation as considered for the full domain simulation, is used for each sub-domain essentially to circumvent the time step limitations The physical domain is split into two equal sub-dimains as shown in Figure 3 4 It is worth mentioning at this stage that Uzawa's algorithm can accomodate any number of sub-domains without any additional complications However, we restrict ourselves to two-subdomain formulation to make the description mathematically more conceivable

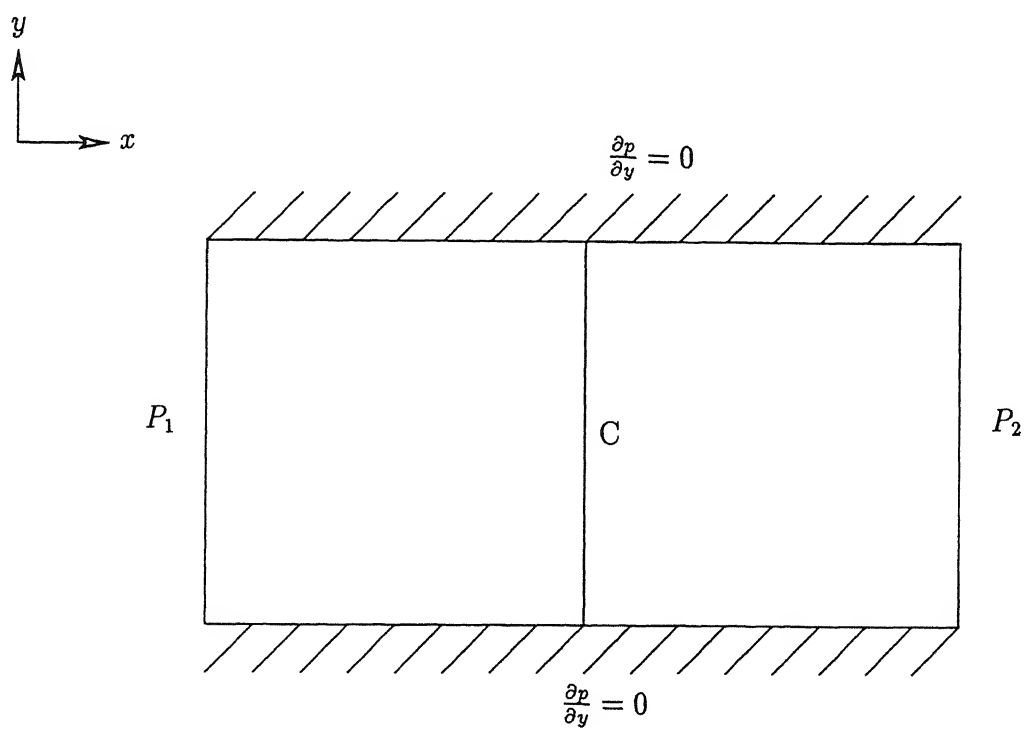

Figure 3 4 Thin Porous Formation Flow Domain and its Division into Two Subdomains

The interface, C, is a straight line parallel to the y-axis This choice of interface saves a considerable amount of effort that will be required while calculating the derivatives of the dependent variables along the outward drawn normal Thus for the sub-domains 1 and 2, boundary conditions on three edges are automatically prescribed from the original problem and only the interface has to be taken care of We solve the pressure equations for the phase pressures, p_o and p_w, in each sub-domain, also to be specially mentioned that the problem is highly non-linear Hence the quantities to be matched at the interface are the phase pressures, p_o and p_w and the Darcy velocities of oil and water This is in analogy with flux matching as described in Section 3 6 3 The Darcy velocities are, $\left(-\frac{kk_{ro}}{\mu_o}\right)\left(\frac{\partial p_o}{\partial x}\right)$ and $\left(-\frac{kk_{rw}}{\mu_w}\right)\left(\frac{\partial p_w}{\partial x}\right)$ Since K and μ are constants with respect to the phase pressures of oil and water, considered as Newtonian fluids, we are essentially left with pressure fluxes, $-k_{ro}\left(\frac{\partial p_o}{\partial x}\right)$ and $-k_{rw}\left(\frac{\partial p_w}{\partial x}\right)$, to be matched at the interface Derivatives with respect to x are calculated along the outward normal at the interface for each sub-domain A brief outline of the algorithm used in the present study is furnished below

(1) At the beginning of each time step, we supply the guess values of the pressure fluxes at the interface The most justified choice would be the fluxes calculated in the previous time step Let us call them λ_o^1 and λ_o^1

(2) With the chosen values of λ_o^1 and λ_o^1, we solve the pressure equations in sub-domains 1 and 2 using λ_o^1 and λ_w^1 as the boundary conditions at the interface Let the solutions be p_{o1}^1 and p_{w1}^1 in sub-domain 1 and p_{o2}^1 and p_{w2}^1 in sub-domain 2

(3) Using Uzawa's algorithm, we update the fluxes as

$$\lambda_o^2 = \lambda_o^1 + \omega\left(p_{o2}^1|_C - p_{o1}^1|_C\right)$$

$$\lambda_w^2 = \lambda_w^1 + \omega\left(p_{w2}^1|_C - p_{w1}^1|_C\right)$$

where, ω is the interface convergence parameter

(4) Steps 2-3 are repeated until the conditions

$$\left|\lambda_o^{I+1} - \lambda_o^I\right| \leq \delta$$

$$\left|\lambda_w^{I+1} - \lambda_w^I\right| \leq \delta$$

are satisfied Here, I indicates the level of interface iteration and δ indicates the con-

vergence limit for interface iterations
(5) Using the pressure values calculated in sub-domains 1 and 2, S_w is updated and *ppv* is calculated
(6) Fresh computation is then started for the next time step and the sequence of operations, steps 1-5, is repeated

3.7 Smoothening of Initial Conditions

The initial conditions for p_o, p_w, S_w and T have been smoothened out to avoid computational instabilities resulting from a step like initial condition However, these spurious oscillations are observed for short times when initial conditions are not smooth Initial conditions are of the form given below

For the thin porous formation domain of nominal size (10 m $\times$ 1 2 m) and grid size (101 $\times$ 11), the initial conditions are as follows

$$\begin{aligned} p_w(x,y) &= (260\,0 - 70\,x) \text{ psi} && 0 \leq x \leq 0\,1\,X \\ &= 190 && 0\,1\,X < x \leq X \end{aligned}$$

$$\begin{aligned} S_w(x,y) &= (0\,86 - 0\,66\,x) \text{ psi} && 0 \leq x \leq 0\,1\,X \\ &= 0\,2 && 0\,1\,X < x \leq X \end{aligned}$$

$$\begin{aligned} T(x,y) &= (100\,0 - 125\,x) \text{ psi} && 0 \leq x \leq 0\,1\,X \\ &= 50\ ^\circ\text{C} && 0\,1\,X < x \leq X \end{aligned}$$

The initial conditions, for the thick porous formation (the two-spot model) domain with a nominal size of (6 m $\times$ 6 m) and grid size of (61 $\times$ 61), for isothermal injection only can be summed up as below

$$\begin{aligned} p_w(x,y) &= (260\,0 - 116\,6\,x) \text{ psi} && 0 \leq x \leq 0\,1\,X \\ &= 190 && 0\,1\,X < x \leq X \end{aligned}$$

$$\begin{aligned} S_w(x,y) &= (0\,86 - 1\,1\,x) \text{ psi} && 0 \leq x \leq 0\,1\,X \\ &= 0\,2 && 0\,1\,X < x \leq X \end{aligned}$$

In this work, we have implemented the domain decomposition technique only for isothermal injection and for the thin porous formation domain of nominal size (4 m × 0 8 m) and grid size of (81 × 5) However, the initial conditions for the same are as follows

$$\begin{aligned} p_w(x,y) &= (260\ 0 - 175\ x)\ \text{psi} && 0 \le x \le 0\ 1\ \text{X} \\ &= 190 && 0\ 1\ \text{X} < x \le \text{X} \end{aligned}$$

$$\begin{aligned} S_w(x,y) &= (0\ 86 - 1\ 65\ x)\ \text{psi} && 0 \le x \le 0\ 1\ \text{X} \\ &= 0\ 2 && 0\ 1\ \text{X} < x \le \text{X} \end{aligned}$$

3.8 Code Validation

The correctness of the computer code has been tested by solving linear and non-linear transient heat conduction equations The matrix obtained from the pressure equations has been solved by both the specialized sparse matrix solver based on Gaussian elimination and by preconditioned conjugate gradient method and the results are seen to be matching quite perfectly Also the code has been tested for various grids The domain decomposition code has been written in such a manner that it can be parallelized without major modifications Calculations in sub-domains are performed in separate subroutines and a main program invokes them and performs the necessary operations The main program has been written in a versatile manner so that it can accomodate as many sub-domains as possible

3.9 Typical Computer Requirements

In the present study all the runs have been taken on a Dec-Alpha 255/233 workstation The isothermal version of the code took around 1 hour and 20 minutes of CPU time for a real time simulation of 3 hours for the thin porous formation flow domain and a time step ($\triangle t$) of 0 01 hour For the same flow domain and for three hour simulation, the non-isothermal version of the code took approximately 1 hour of CPU time for a time step ($\triangle t$) of 0 005 hour The isothermal version of the code for the two-spot problem took around 2 hours of CPU time for a simulation of three hours and a time step $\triangle t$ of 0 01 hours The convergence criteria used was $(Q^{p+1} - Q^p)/Q^{p+1} \times 100 < 0\ 01$, where, Q is p_o, p_w and T for all the above cases

Chapter 4

Results and Discussions

In this chapter the results have been grouped under the following sections
(1) Results related to the flow domain of thin porous formation for both isothermal and non-isothermal injection and the effect of surfactants for isothermal injection,
(2) Various numerical issues corresponding to the domain decomposition technique applied to the flow domain of thin porous formation, and
(3) Results in correspondance with the thick porous formation flow domain i e for the two-spot model

4.1 Results for the Thin Porous Formation Flow Domain

The following issues have been discussed in this section

1 Effect of formation temperature (T_f) on oil displacement efficiency (ppv)

2 Comparison of oil recovery for the isothermal and non-isothermal cases for a given value of T_f

3 Evolution of saturation and temperature profiles for the isothermal and non-isothermal cases

4 Effect of heat loss, to the overhang and underhang, on oil recovery

5 Effect of surfactants on oil recovery

4.1.1 Isothermal Injection

Figure 4 1 shows the rise in saturation level of water in the flow domain along its centreline with time There is no front and the profile is diffusion dominated Next, we consider the effect of increasing the formation temperature We find an increase in the water saruration along the centreline of the flow domain as we raise the formation temperature from 30 °C to 50 °C in steps of ten (Figure 4 2) The improvement in oil recovery with the increase in formation temperature has been depicted in Figure 4 3 This is however expected because with the increase in temperature, the oil viscosity decreases, thus resulting in an icrease in the mobility of oil Figure 4 4 shows the pressure profiles for both oil and water

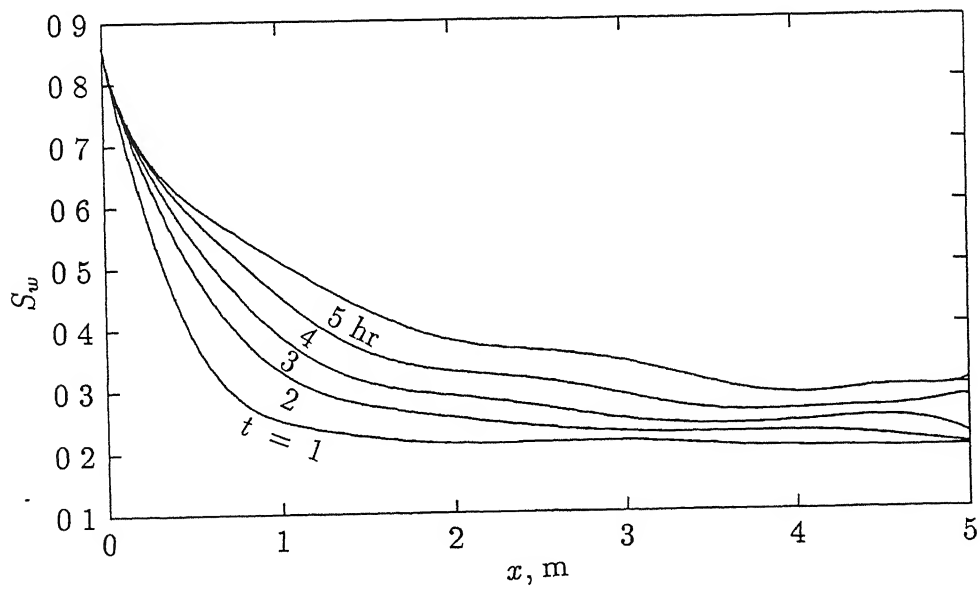

Figure 4 1 Progress of Saturation Front for Isothermal Injection of Water

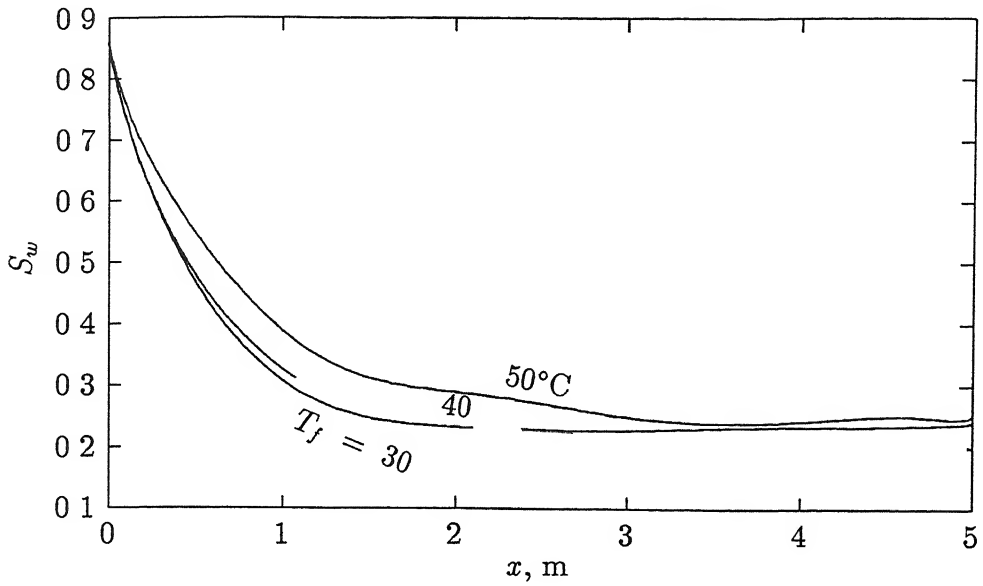

Figure 4 2 Effect of Formation Temperature (T_f) on Saturation Front for Isothermal Injection of Water

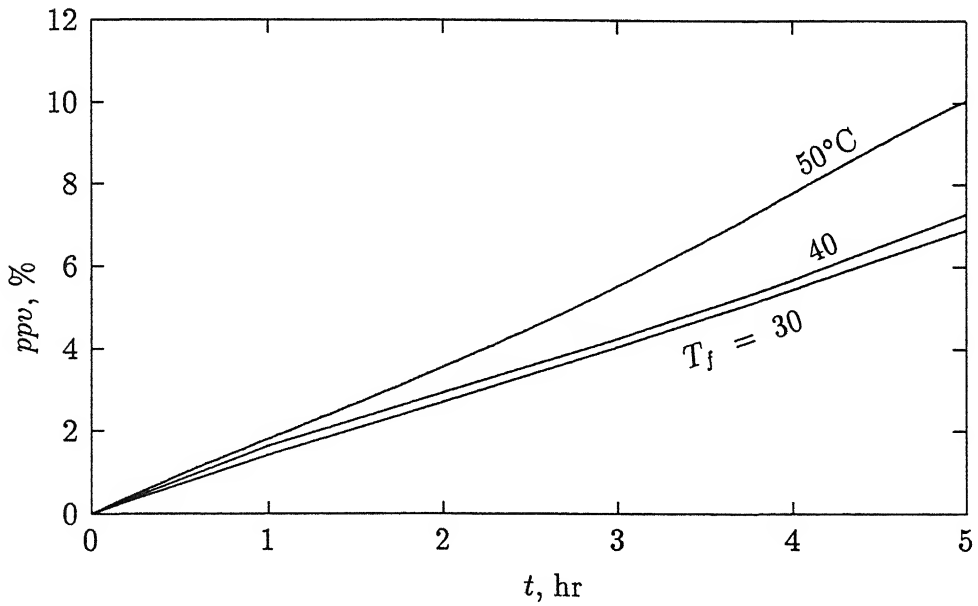

Figure 4 3 Effect of Formation Temperature (T_f) on Oil Displacement Efficiency for Isothermal Injection of Water

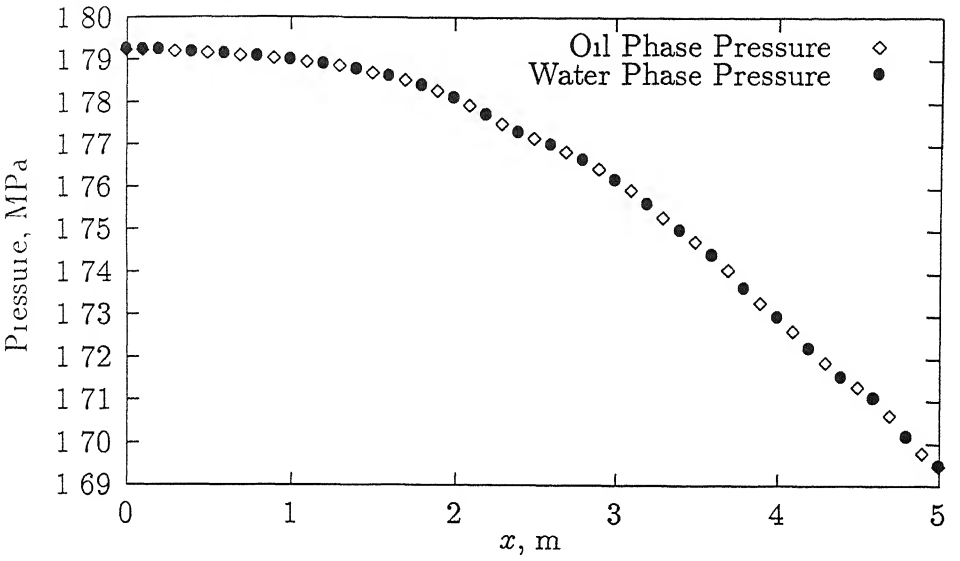

Figure 4 4 Progress of Pressure Fronts of Oil and Water for Isothermal Injection of Water

4.1 2 Oil Displacement Efficiency

Oil displacement efficiencies for the isothermal (cold water injection) and non-isothermal (hot water injection) cases are compared in Figure 4 5 The *ppv* in the non-isothermal case is seen to be below that of the isothermal case A possible explanation to this is that the accumulation of oil ahead of the water saturation front in the non-isothermal case increases the overall formation resistance However, this phenomenon is not present in the isothermal case The phenomenon leads to an overall decrease in the oil displacement efficiency for non-isothermal injection as compared to the isothermal injection, although the reverse may be expected elsewhere

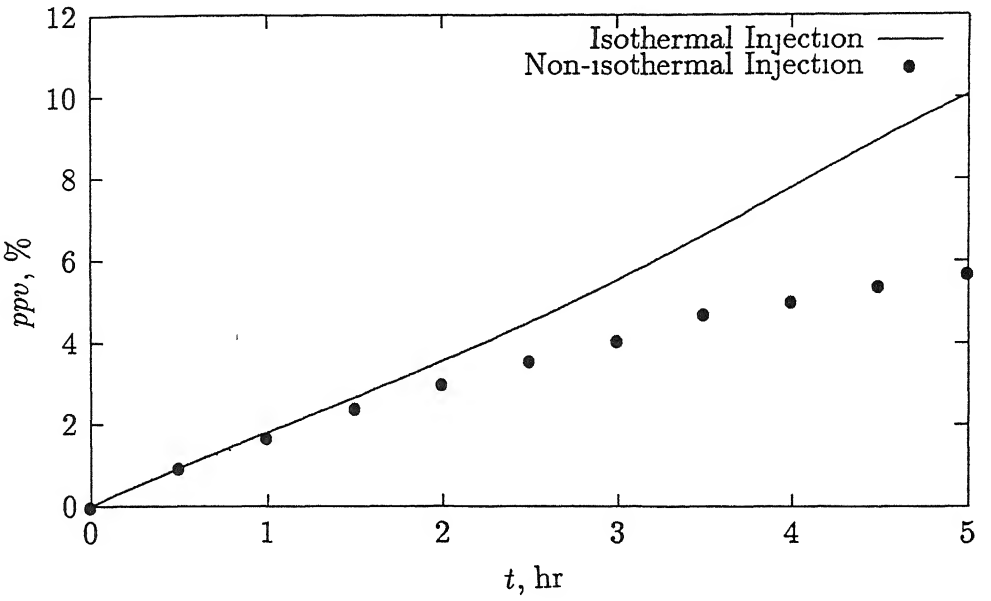

Figure 4 5 Oil Displacement Efficiency as a Function of Time for Isothermal and Non-isothermal Injection of Water

4.1.3 Non-isothermal Injection

The results due to the hot water injection technique are discussed in this subsection Figures 4 6 and 4 7 show the development of centreline saturation and temperature profiles respectively Both of them reveal a distinct front like structure and on comparing them, we see that the saturation front moves more or less with the same speed as the temperature front The saturation profile shows an unusual dip immediately beyond the front A possible explanation may be that in the vicinity close to the injection zone, due to the temperature front the viscous resistance decreases appreciably and the capillary resistance is also not very high It essentially increases the waterflood. But in the downstream region, both viscous resistance and capillary resistance predominate and an appreciable drop in the water saturation values is found Figure 4 8 shows the progress of pressure fronts for oil and water phase pressures The oil and water pressures drop steadily after a distance of 1 2 m from the injection well

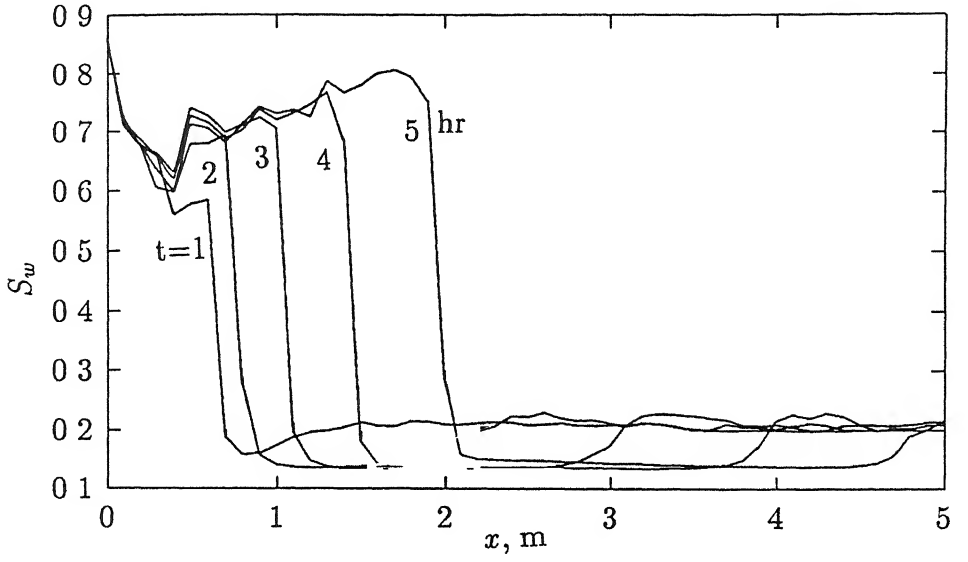

Figure 4 6 Progress of Saturation Front for Hot Water Injection

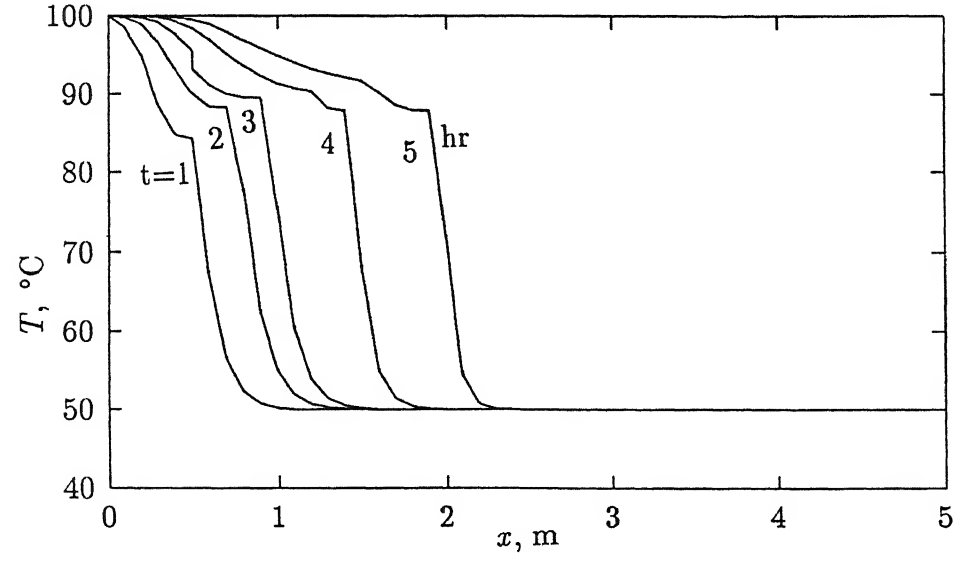

Figure 4 7 Progress of Temperature Front for Hot Water Injection

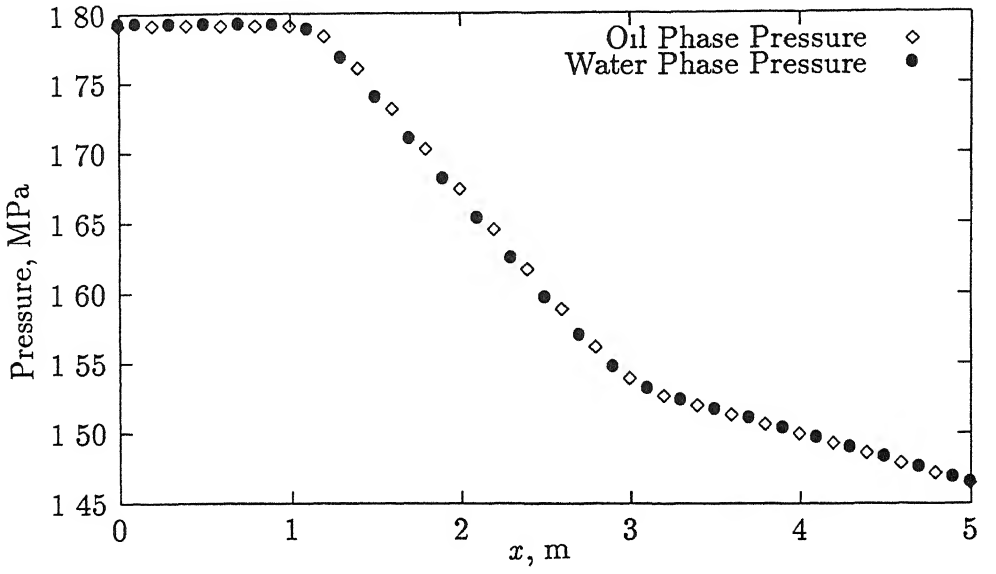

Figure 4 8 Progress of Pressure Fronts of Oil and Water for Hot Water Injection

4.1.4 Effect of Heat Loss

The effect of heat loss to the overhang and the underhang on oil recovery has been discussed in this subsection The pertinent parameter which helps in determining the heat loss is Biot number, Bi The higher the value of Bi, the greater is the heat loss Since convection plays a dominant role in the transportation of oil, the effect of heat loss does not influence the centreline characteristics significantly for the given domain width (Y = 1 2 m) and for the time-frame considered here Figure 4 9 shows the typical widthwise temperature profiles for various values of Bi For Bi = 0 0 and 0 01, the profiles are straight lines, which implies that the overhang and the underhang are perfect insulators The profile for Bi = 1 is more or less a straightline and shows up quite significant insulation effect But for increasing values of Bi from 100 to 10000, the profile becomes increasingly parabolic in nature The slopes show maxima at the top and the bottom of the domain, because of the heat loss to the host rocks This effect is dominant near the region very close to the injection zone However, in further downstream the effect has been seen to be significantly small or not found at all In the figure, the results have been given for a distance of X = 1 25 m from the injection zone

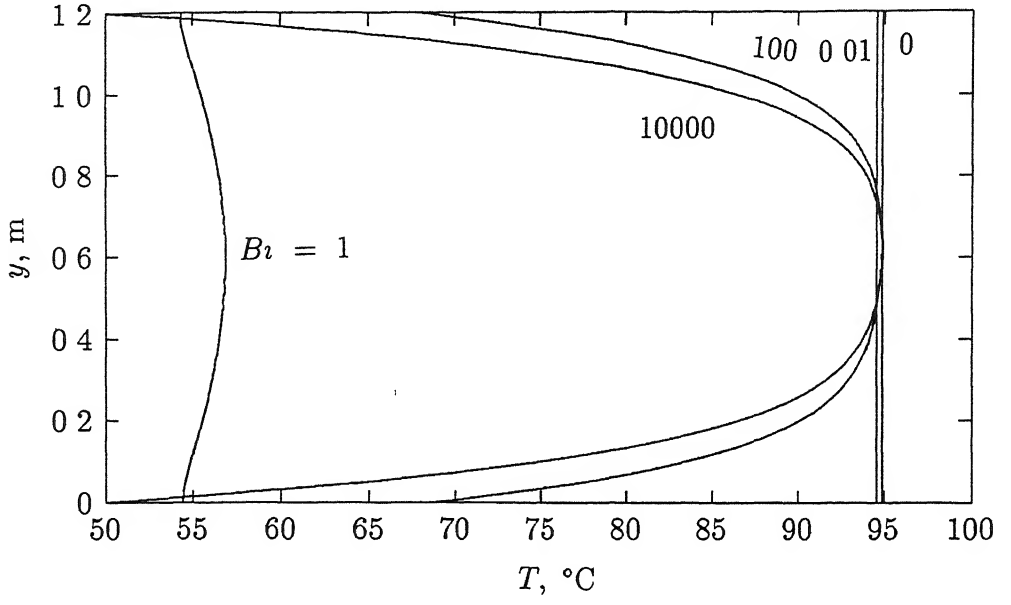

Figure 4 9 Effect of Bi on Widthwise Temperature Profile for Hot Water Injection

4.1.5 Effect of Surfactants

The effect of surfactant flooding on oil recovery has been explained in this subsection Figure 4 10 shows the oil recovery in terms of *ppv* as a function of the formation temperature The two cases, namely, injection without surfactants and with surfactants have been compared here It is seen that *ppv* increases with temperature This is because an increase in formation temperature lowers the oil viscosity and hence enhances the mobility of oil-water bank The decrease in surface tension in the presence of surfactants is also clear in the figure As a consequence, the increase in oil recovery in the presence of surfactants is quite appreciable as compared to that without surfactants Figure 4 11 compares water saturation profiles after three hours of injection with and without surfactants It is seen that both the profiles are influenced by the diffusion However, the saturation curve for injection with surfactants always shows higher values than that for injection without surfactants Thus, a greater mobility of the oil-water bank in the presence of surfactants is ascertained Figure 4 12 shows the pressure profiles for oil and water for isothermal injection with surfactants The pressure drop for both the components is gradual

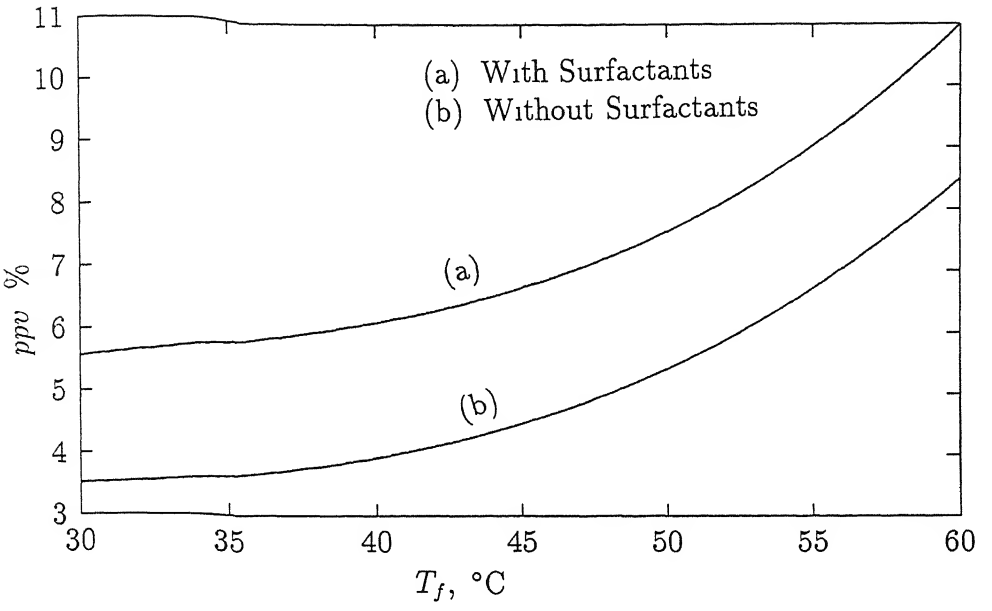

Figure 4 10 Oil Displacement Efficiency as a Function of Formation Temperature (T_f) for Isothermal Injection of Water with and without Surfactants

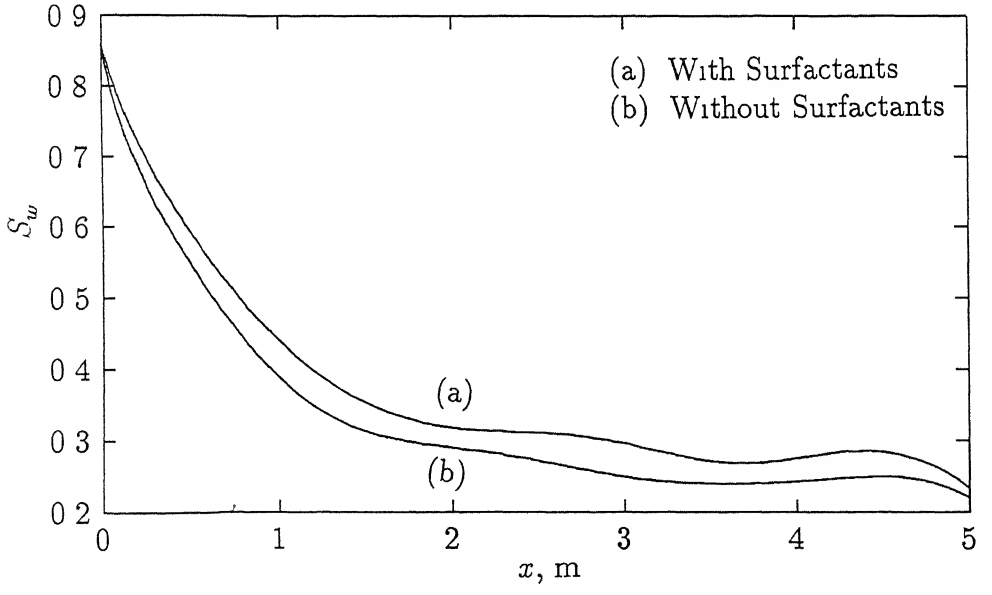

Figure 4 11 Variation of Water Saturation with Distance at the End of Three Hours for Isothermal Injection of Water with and without Surfactants

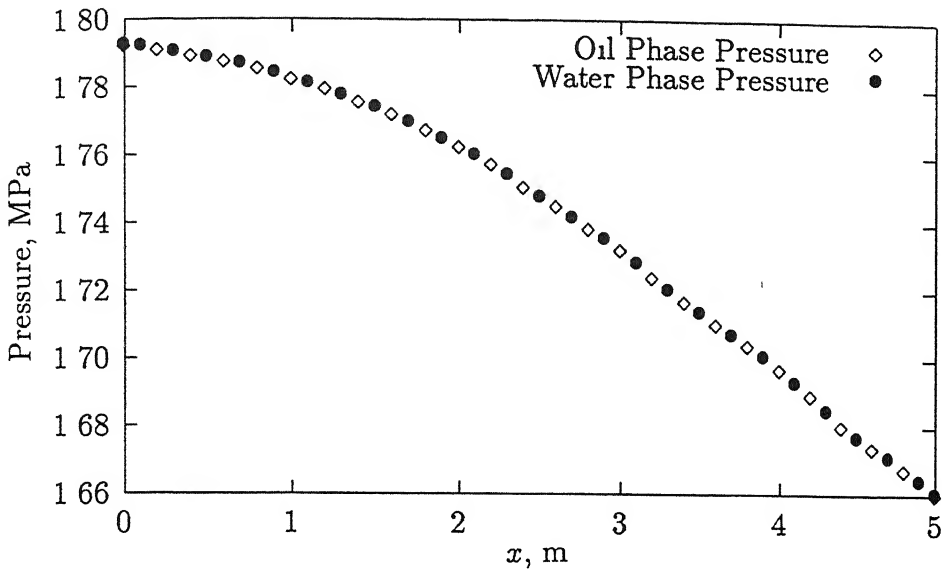

Figure 4 12 Progress of Pressure Fronts of Oil and Water for Isothermal Injection of Water with Surfactants

4.1.6 Application of PCG Method

The preconditioned conjugate gradient method (PCG) has been applied to solve the matrix arising out of the pressure equations for the hot water injection case Figures 4 13 and 4 14 show the comparison of the saturation and temperature fronts, predicted by the PCG and by the Gaussian Elimination, respectively The results are seen to be matching almost perfectly This comparison serves to establish the accuracy of the individual solution techniques

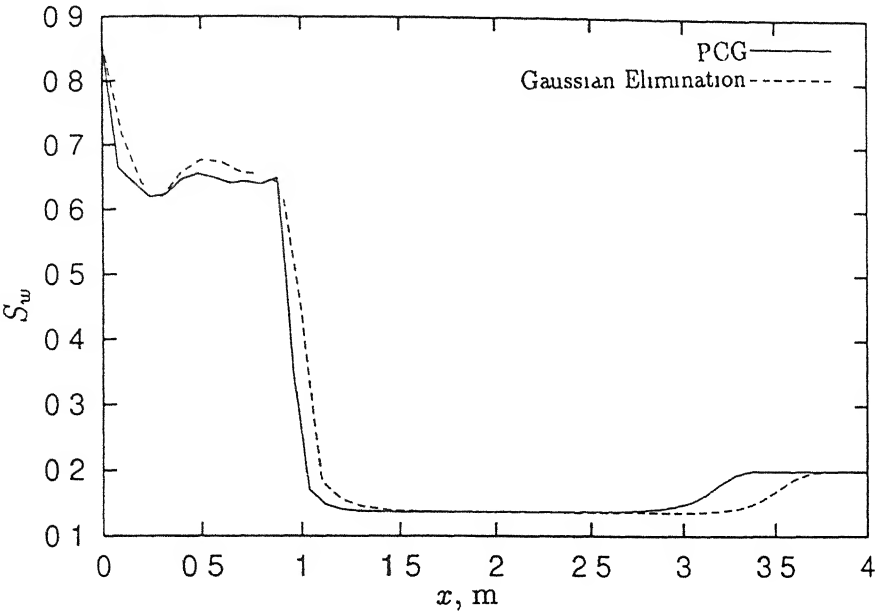

Figure 4.13 Comparison of Saturation Front Predicted by PCG and Gaussian Elimination

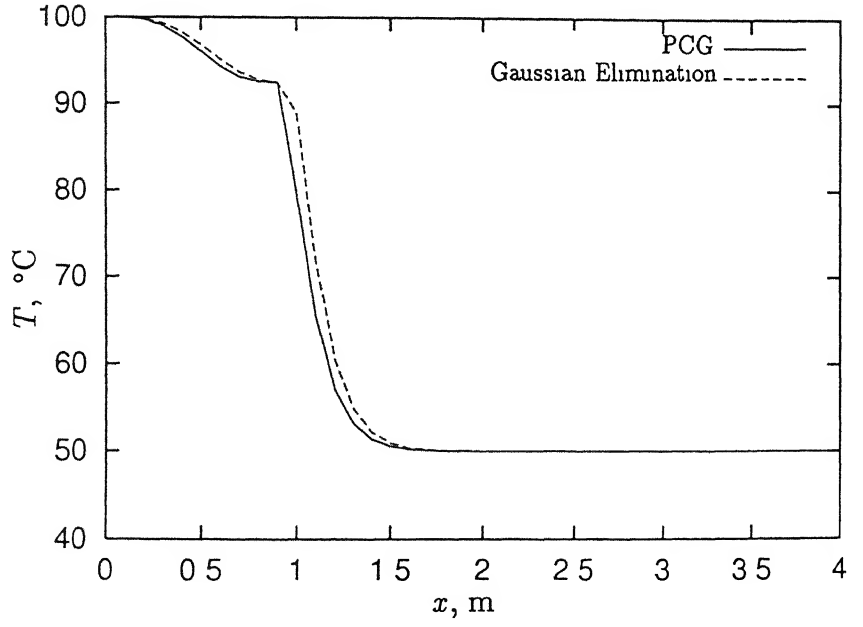

Figure 4.14 Comparison of Temperature Front Predicted by PCG and Gaussian Elimination

4.2 Numerical Issues Regarding Domain Decomposition

Various numerical issues related to the domain decomposition technique applicable to the simulation of flow through the thin porous formation have been discussed herein

Table 4 1 compares the saturation values calculated using the full domain simulation and the simulation with domain decomposition The values are seen to be sufficiently close at various distances from the injection zone Table 4 2 shows the comparison between the CPU times taken for five hour simulation using the full domain simulation and the domain decomposition code Domain decomposition is seen to take more CPU time This can be attributed to the use of a sequential machine in solving a highly non-linear problem Implementation of parallelization is expected to show an overall speed up of the computing time Also to be mentioned that for the linear problems, domain decomposition has been found to be faster even on sequential machine For both the cases, the formation temperature is 30°C and the domian decomposition algorithm has been applied for two sub-domains

Table 4 1. Comparison of Saturation Values for Full Domain Simulation and Simulation with Domain Decomposition

	x, m	0 5	1 0	1 5	2 0	2 5	3 0	3 5	4 0
$t = 3$ hr	A*	0 3595	0 2837	0 2589	0 2538	0 2016	0 2009	0 2113	0 2000
	B†	0.3513	0 2789	0 2617	0 2420	0.2717	0 2451	0 2175	0 2004
$t = 5$ hr	A*	0.4585	0 3379	0 3287	0 2872	0 2637	0 2404	0 2585	0 2000
	B†	0 4500	0 3355	0 3214	0 2916	0 2578	0 2300	0 2138	0 2004

* Full domain simulation

† Simulation with domain decomposition

Table 4 2 Comparison of CPU Time Values for Full Domain Simulation and Simulation with Domain Decomposition

	CPU time
A	130 seconds
B	3560 seconds

* Full domain simulation

† Simulation with domain decomposition

4.2.1 Effect of Interface Convergence Parameter

Here we are discussing the effect of interface convergence parameter (ω) on domain decomposition We know that ω is an adjustable constant that lies between 0 and 1 In the present work we have performed a thorough numerical experimentation to find out an optimum value of ω However, the subsequent text shows a comparative study for three values of the interface parameter (ω = 0 2, 0 25 and 0 3) based on the CPU time taken for a five hour simulation (Table 4.3) Also, the *ppv* values at the end of five hours with respect to different ω values have been compared with the results due to full domain simulation (Table 4 4)

Table 4 3. Comparison of CPU Time Values

	CPU time
ω = 0 2	3800 seconds
ω = 0 25	3560 seconds
ω = 0 3	3900 seconds
FDS‡	130 seconds

‡ Full Domain Simulation

Table 4 4 Comparison of *ppv* Values

t, hr	1	2	3	4	5
$\omega = 0\ 2$	2 5447	4 9307	7 8495	10.016	12 739
$\omega = 0\ 25$	2 8382	5 0785	7 2961	10 168	11 911
$\omega = 0\ 3$	2 8369	5 1859	7 8202	10.110	12.083
FDS‡	2 8299	5 3882	7 7988	10 175	12.536

‡ Full Domain Simulation

From the above comparison, it is clear that the *ppv* values for $\omega = 0\ 25$ and 0.3 are very close to that obtained from the full domain simulation. But the CPU time for $\omega = 0\ 25$ is less than that for $\omega = 0\ 3$. For the problem of interest, we have identified that $\omega = 0\ 25$ is the optimum value and all the calculations concerning the domain decomposition technique have been done based on that value.

4.2.2 Effect of Uzawa Convergence Limit

The effect of convergence limit for the interface iterations on the simulation with domain decomposition as compared to the full domain simulation has been discussed in this subsection Figures 4 15 and 4.16 show the pressure profiles for oil and water respectively for two values (10^{-3} and 10^{-4}) of the Uzawa Convergence Limit (hereafter UCL) and those for the full domain simulation For both the cases, the interface convergence parameter (ω) is 0 25 and the formation temperature is 30°C. The figures clearly show that for a lower value of the UCL, the pressure profiles are closer to those obtained from the full domain simulation. It will obviously predict a much better *ppv* value at the end of five hour simulation as it is observed from the Table 4.5. Table 4 5 shows a comparison of the *ppv* values for simulation with domain decomposition for the two UCL values and the full domain simulation

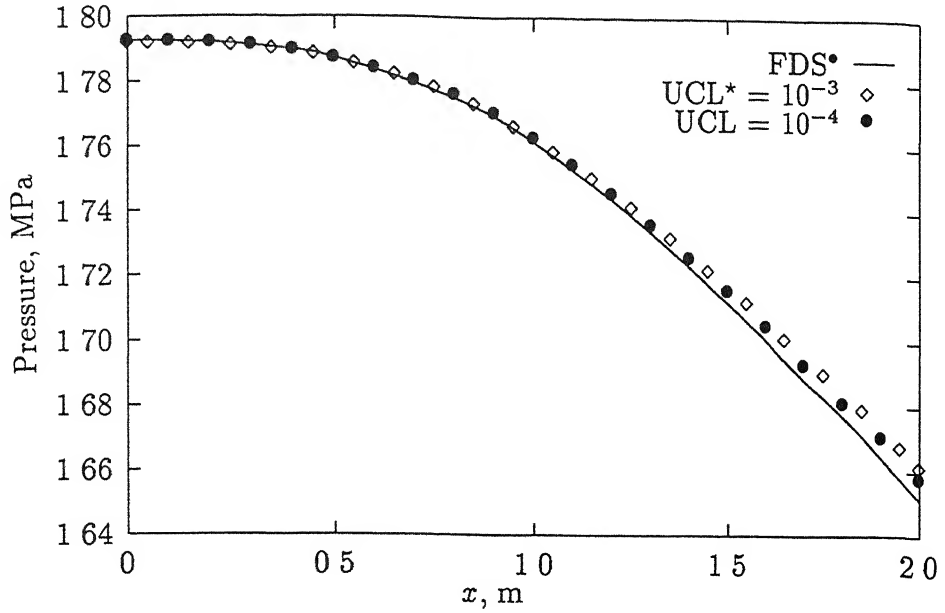

Figure 4 15 Comparison of Oil Pressure Profile for Various Values of Uzawa Convergence Limit and for Full Domain Simulation

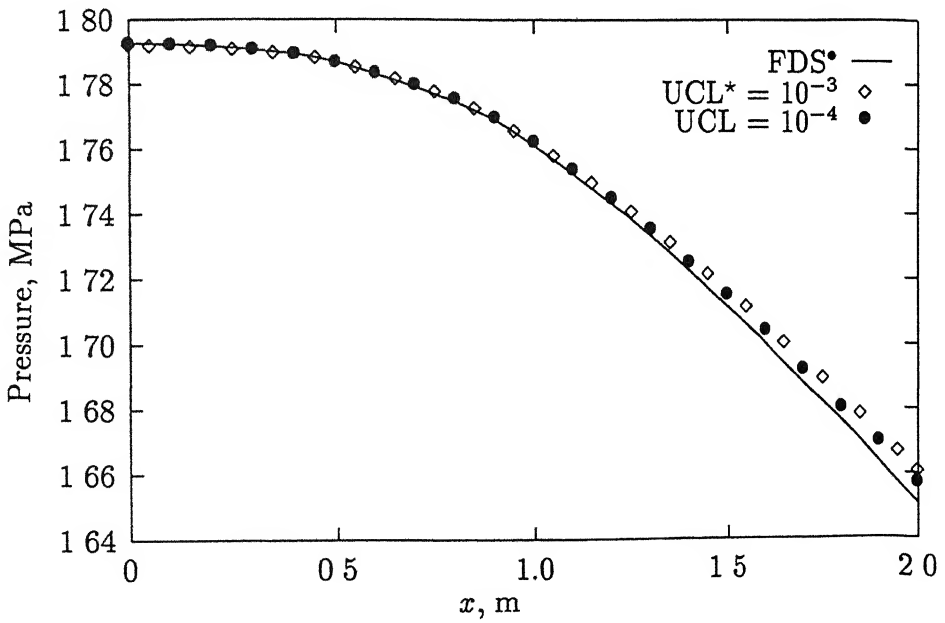

Figure 4 16 Comparison of Oil Pressure Profile for Various Values of Uzawa Convergence Limit and for Full Domain Simulation

Table 4 5. Comparison of *ppv* Values

	ppv
UCL* $= 10^{-3}$	11.911
UCL $= 10^{-4}$	12 208
FDS•	12 536

* Uzawa Convergence Limit
• Full Domain Simulation

4.2.3 Effect of Interface Treatment

This subsection discusses the effect of various interface treatments on simulation with domain decomposition. In the present study, we have considered a variant of three interface treatment approaches In the first approach, we have taken only one-sided normal derivative of the phase pressure gradients at the interface In the second approach, we have considered the averaging of the normal derivatives of the phase pressure gradients at the interface However, both the approaches give very close *ppv* values for a five hour simulation, as shown in Table 4.6. In both the cases, the phase pressure gradients are used as the initial guess for the interface condition and are updated subsequently through Uzawa iterations. Therefore, the final solution does not change In the third approach, we have used the mass fluxes, derived from the Darcy's law (as discussed in Section 3.6.4), instead of the pressure gradients However, due to some unidentified difficulties experienced in implementing the mass flux approach, we are unable to furnish any result here. The failure forms a strong motivation for the future work using the mass-flux based interface-treatment. In the first and second approaches, we have taken $\omega = 0.25$, $T_f = 30°C$ and UCL $= 10^{-3}$

Table 4 6: Comparison of *ppv* Values

	ppv
FA◇	11 911
SA⊙	12.022

◇ First Approach
○ Second Approach

4.3 Results for the Two-spot Model

In this section, various issues related to the simulation of the two spot model have been discussed Results for the three simplified versions (Figures 2 2 (c), (d) and (e)) of the original two-spot model (2 2 (b)) have been presented here

4.3.1 Oil Displacement Efficiency

Figures 4 17, 4 18 and 4 19 show the oil displacement efficiencies for the isothermal injection with and without surfactants The *ppv* values are seen to be higher for injection with surfactants This is expected as surfactants reduce the surface tension effect, thus enhancing the mobility of the oil-water bank Two values of the formation temperature, T_f = 40°C and 50°C, have been considered Figures 4 17 (a), 4 18 (a) and 4 19 (a) show the displacement efficiencies for T_f = 40°C and Figures 4 17 (b), 4.18 (b) and 4.19 (b) show the displacement efficiencies for T_f = 50°C. However, the figures show that for surfactant flooding (for the cases corresponding to Figure 2.2 (c) and Figure 2 2 (e)), it was not possible to go for full five hour simulation. A possible explanation behind this peculiar phenomenon is that surfactants enhance the mobility of the oil-water bank to such an extent that from some regions in the flow domain oil is fully flushed out and only water remains This implies that after a few hours of simulation, in some regions the water saturation, S_w becomes 1. In other words, oil saturation, S_o tends to 0. Our model is not valid for such a situation. We assume that the irreducible limit for oil is S_w = 0 86 and that for water is S_w = 0.1 Therefore, for the simulation of surfactant flooding, we require to choose the formation temperature in such a way that the irreducible limit is not overlooked It may be mentioned that full five hour simulation was accomplished for the case corresponding to Figure 2.2 (d) and the formation temperature, T_f = 40°C (see the results in Figure 4.18 (a))

4.3.2 Transverse Pressure Profile

Figures 4 20, 4.21 and 4.22 show the evolution of the transverse pressure profiles for the flow domains as shown in Figures 2.2 (c), (d) and (e) respectively. The profiles are seen to exhibit a gradual increasing trend in slope along the y direction. This is, however,

expected for the sustenance of the flow of oil from the injection well to the production well For all the above three cases the formation temperature has been taken as 50°C and isothermal injection without surfactants has been considered Figures 4 20 (a), 4 21 (a) and 4 22 (a) show the pressure profiles for the oil phase and Figures 4 20 (b), 4 21 (b) and 4 22 (b) show the pressure profiles for the water phase

4.3.3 Saturation Profile

The distribution of saturation (S_w) in the flow domain for the two-spot model has been predicted here Figure 4 23 shows the saturation distribution for the flow domain (corresponding to Figure 2 2 (c)) for various durations of simulation Figure 4 23 (a) shows the initial distribution of S_w while Figures 4 23 (b), 4 23 (c) and 4 23 (d) predict the distribution of S_w after three hours, five hours and ten hours respectively For the other two flow domains (as shown in Figures 2 2 (d) and (e)) more or less same trend of variation of the saturation distribution has been observed However, from the figures, it can be conjectured that S_w increases unusually in the region of the production well for the simulations for three hours, five hours and ten hours This may be due to the intrinsic approximation of the original two-spot model which entails accumulation of water near the impermeable bounding surfaces. However, the accumulation of water in the vicinity of the production well in the present simulation has been unusually high Also here, we have taken the injection and production well diameters as 1 meter while the dimension of the two-spot model flow domain (Figure 2 2 (b)) is only 6 meters But in real life, the two-spot domain size itself may be several times of the domain size considered in the present study This may also lead to unusual behaviour in the saturation distribution

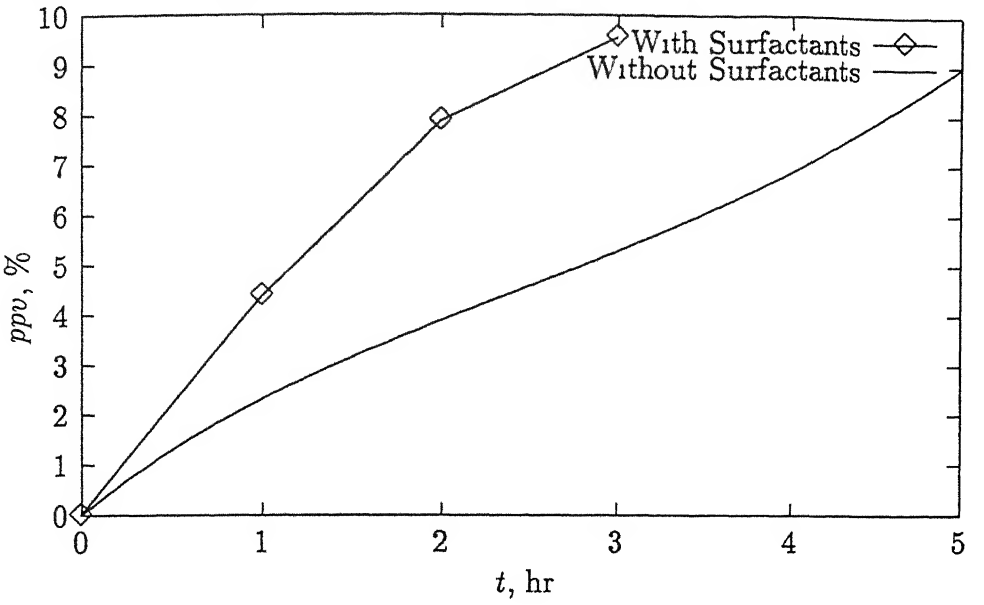

(a)

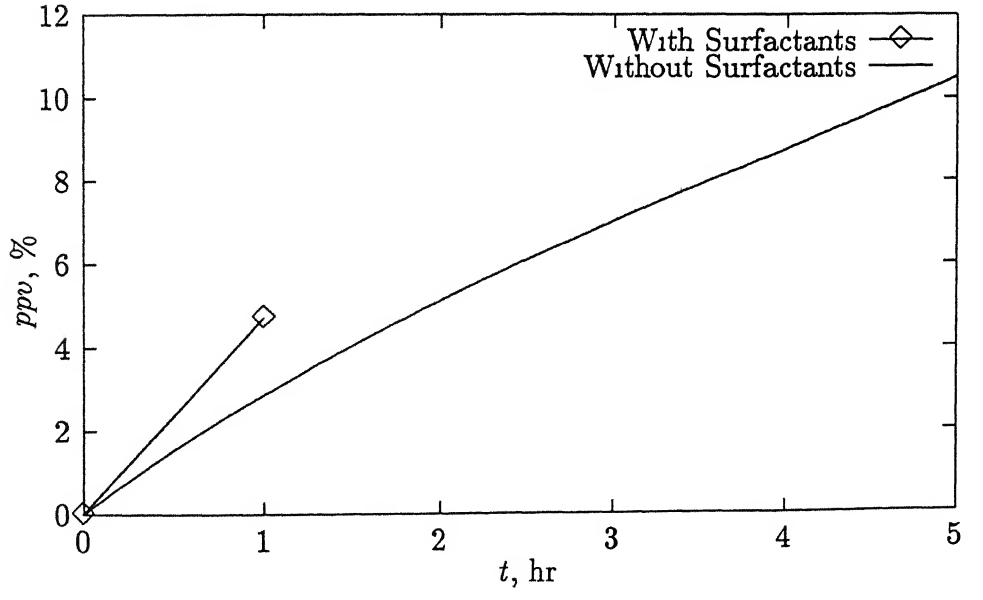

(b)

Figure 4 17 Oil Displacement Efficiency as a Function of Time for Isothermal Injection of Water with and without Surfactants for the Two-spot Model Flow Domain as shown in Figure 2 2 (c)

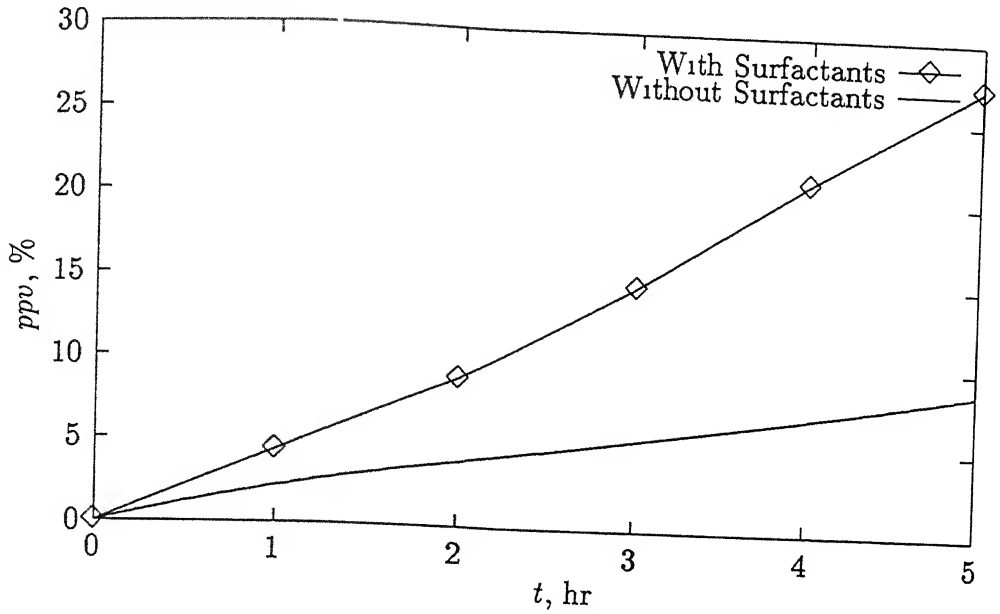

(a)

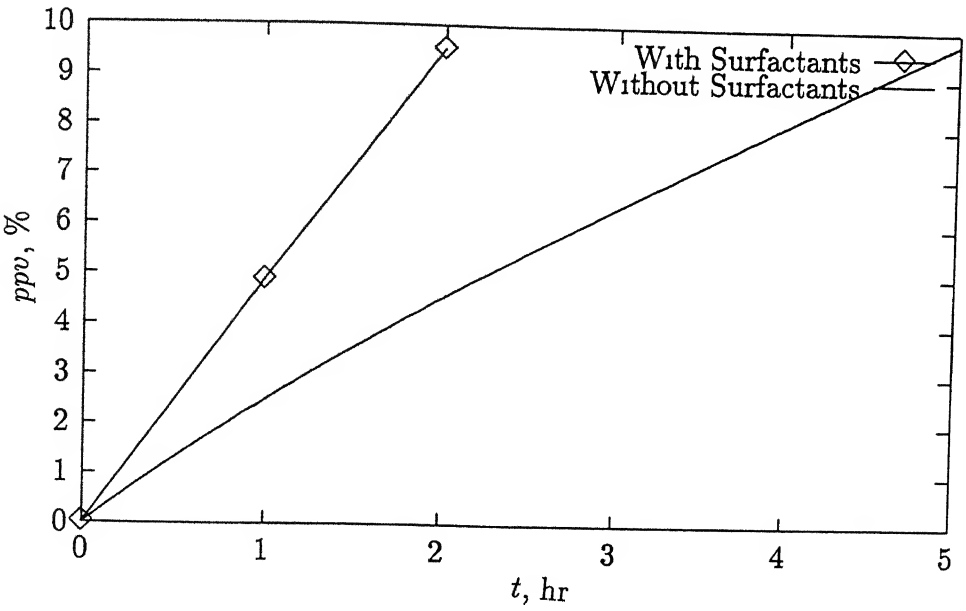

(b)

Figure 4 18 Oil Displacement Efficiency as a Function of Time for Isothermal Injection of Water with and without Surfactants for the Two-spot Model Flow Domain as shown in Figure 2 2 (d)

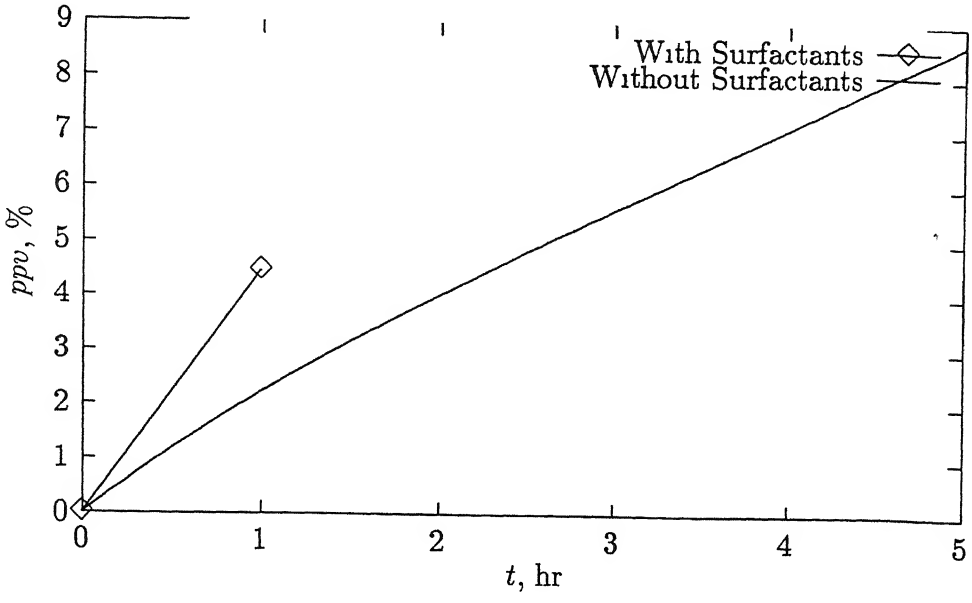

(a)

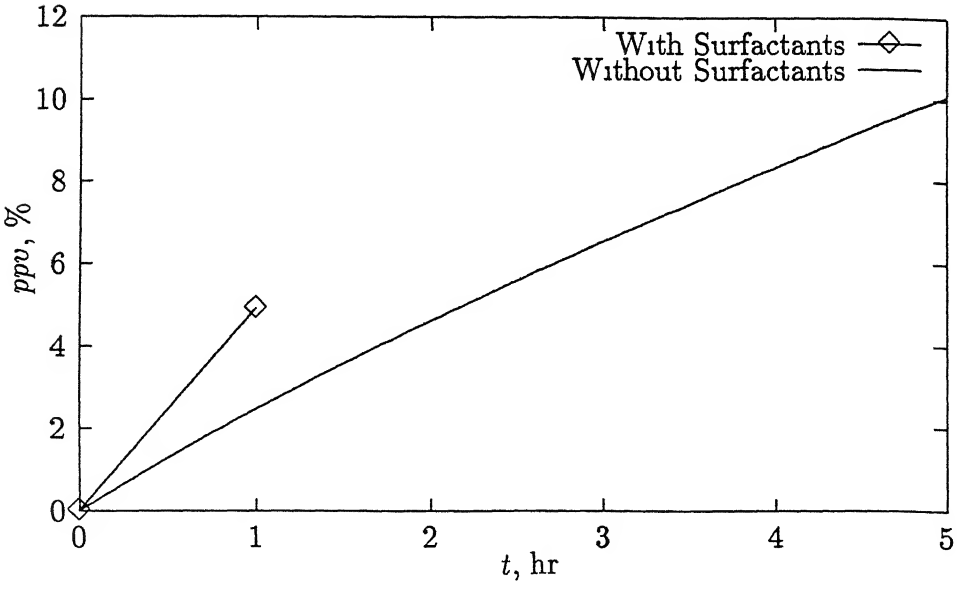

(b)

Figure 4 19 Oil Displacement Efficiency as a Function of Time for Isothermal Injection of Water with and without Surfactants for the Two-spot Model Flow Domain as shown in Figure 2 2 (e)

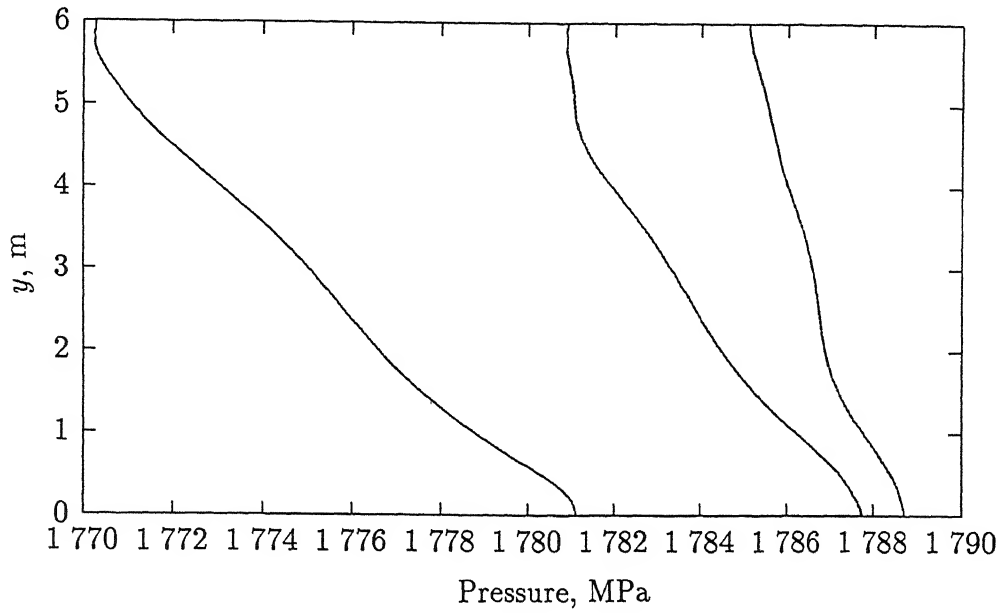

(a)

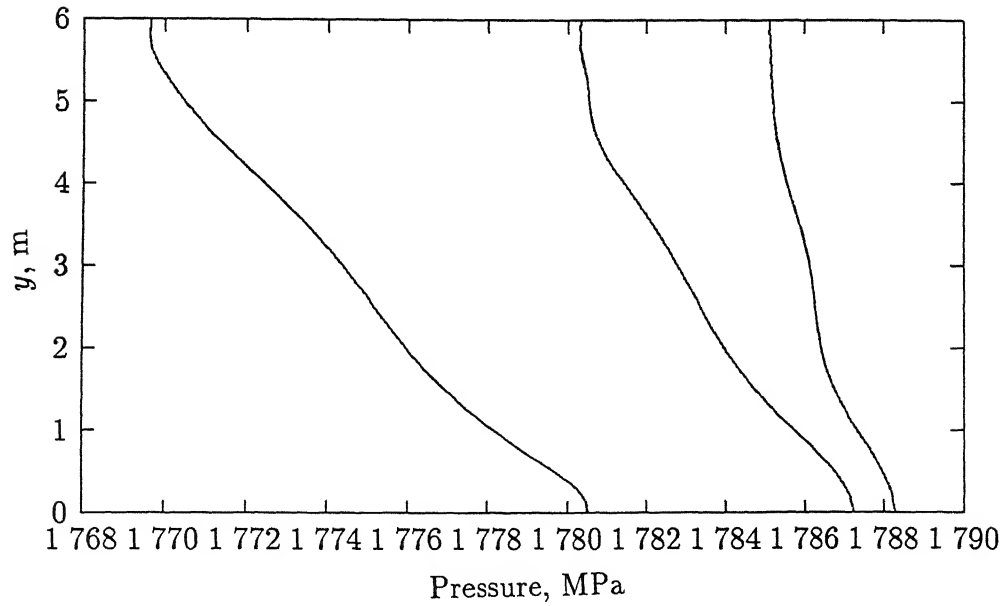

(b)

Figure 4 20 Variation of Transverse Pressure Profiles of Oil and Water for Isothermal Injection of Water without Surfactants for the Two-spot Model Flow Domain as shown in Figure 2 2 (c)

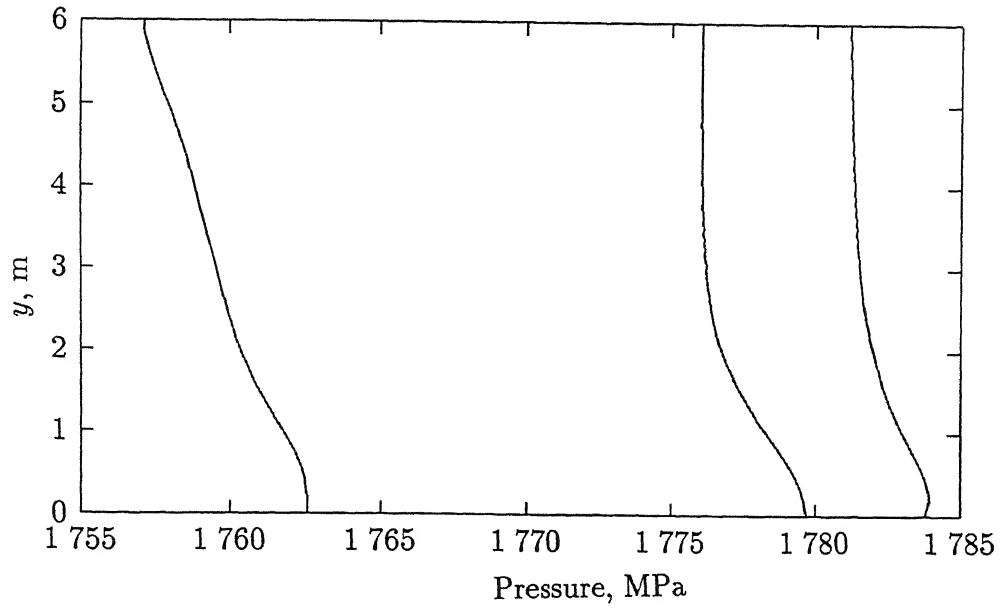

(a)

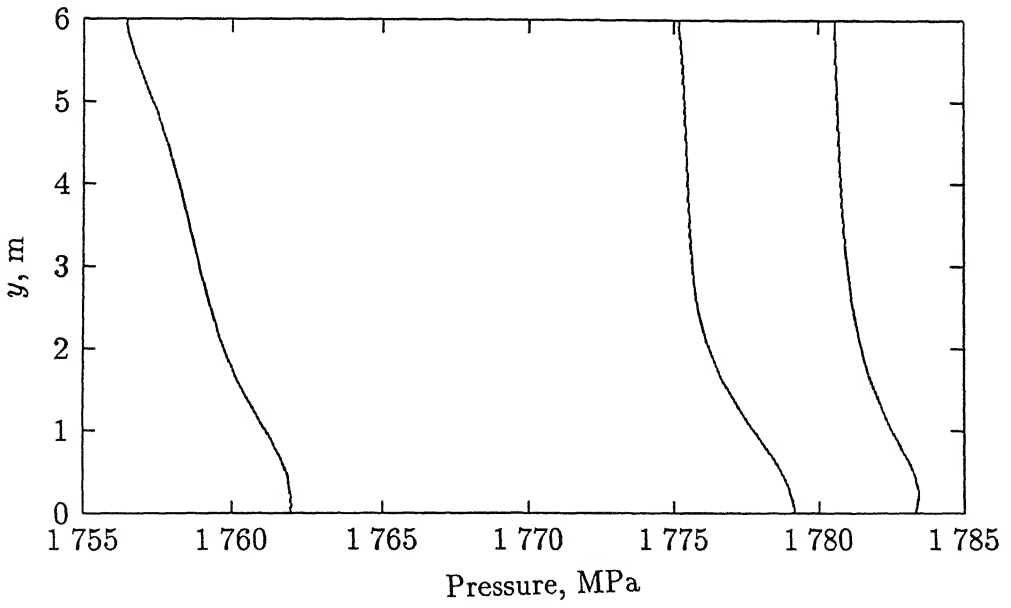

(b)

Figure 4 21. Variation of Transverse Pressure Profiles of Oil and Water for Isothermal Injection of Water without Surfactants for the Two-spot Model Flow Domain as shown in Figure 2 2 (d)

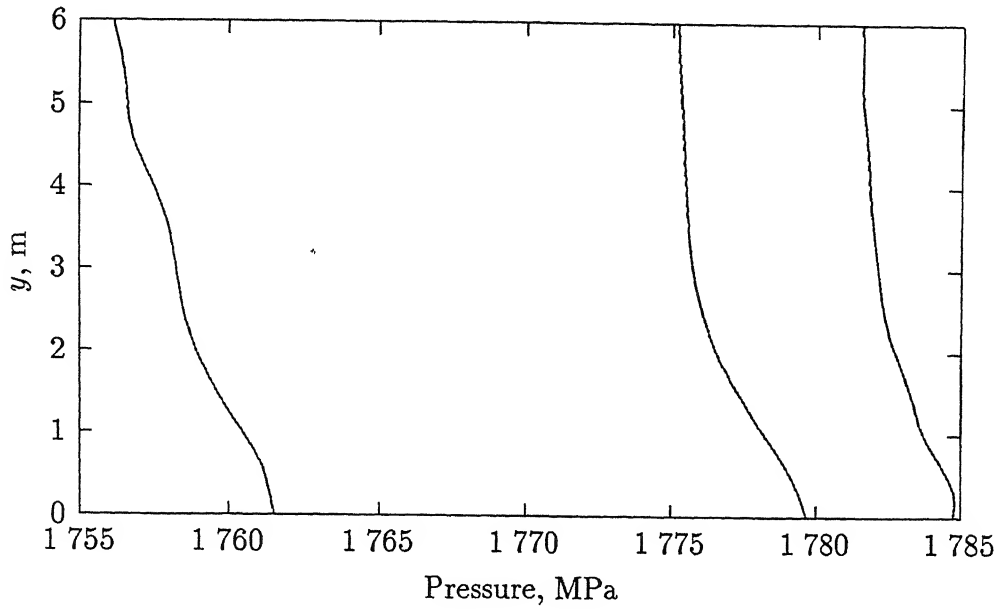

(a)

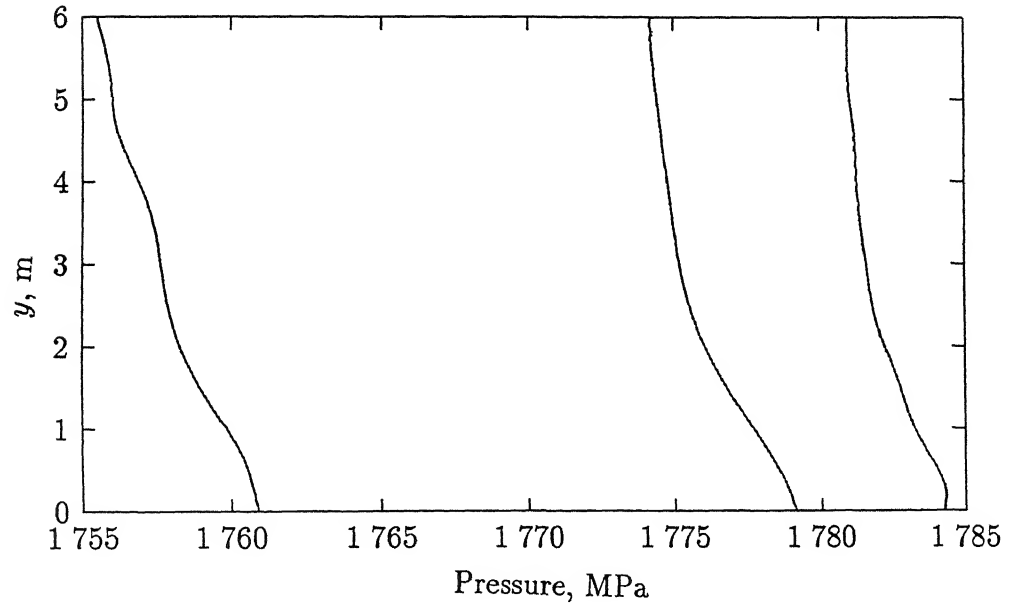

(b)

Figure 4 22 Variation of Transverse Pressure Profiles of Oil and Water for Isothermal Injection of Water without Surfactants for the Two-spot Model Flow Domain as shown in Figure 2 2 (e)

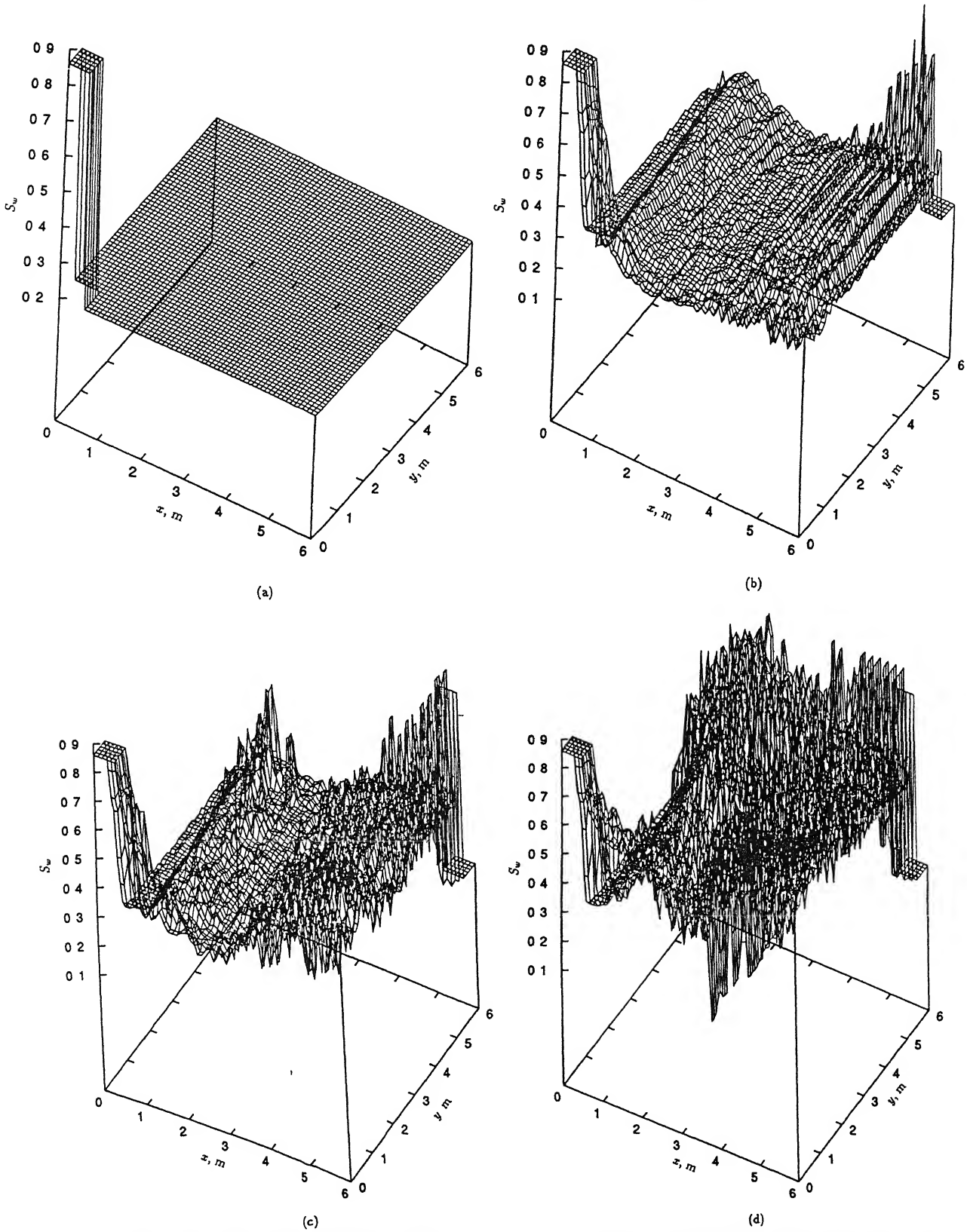

Figure 4 23: Distribution of Water Saturation for the Two-spot Model Flow Domain as shown in Figure 2 2 (c).

4.4 Concluding Remarks

Before concluding, we would like to mention about role of the field data in the form of constitutive relations as furnished in Table A 1 of Appendix A In the table, $k_{r_{o,w}}$ is given for a finite set of S_w values A linear interpolation is used to compute intermediate values of the relative permeability and capillary pressure Also it is well known that the prediction of a numerical simulator for flow through a porous media is sensitive to the values of k_{ro}, k_{rw} and $p_{c_{o,w}}$. Any deviation from the correct values with respect to these input parameters can lead to the unrealistic predictions. However, the pointers from the open literature suggest that the closed form analytical expressions are expected to improve the quality of the numerical predictions (Pruess and Narasimhan, 1982)

Also it is essential to point out the relative advantages of harmonic averaging over arithmetic averaging of θ and γ values as found in the pressure equations (Section 3.1) The reason behind the choice of harmonic averaging is that the viscosity has very sensitive exponential dependence on temperature and the relative permeability changes sharply with saturation The resultant effect can cause sharp variations in θ and γ values in a small region However, the choice proved to be a correct one as the wiggles in saturation profiles for the isothermal case were remarkably reduced in magnitude when the property values were determined using harmonic averaging procedure.

Chapter 5

Conclusions and Scope for Future Work

In this work, we have tried to take up the numerical simulation of the enhanced oil recovery problem from different perspectives. It includes modeling and simulation of flow through two different domains The two-spot problem is a major venture in this study It gives an idea as to how field-scale problems can be tackled The implementation of the domain decomposition technique is yet another attempt to study the oil recovery problem from the stand point of a real reservoir simulation. It forms the building block of simulation of the large reservoirs The implementation of the PCG method in solving the matrix arising out of the pressure equations is another salient feature of the present work and it is a primafacie attempt towards parallelizing the complete code in future

Recommendations

The following extensions to the present work are recommended to make the numerical simulation of the oil recovery problem complete, robust and realistic

(1) **Stability limits of simulation:**

The numerical work presented in this work has been done for one particular formation i e one particular set of formation and surfactant properties Due to high degree of non-linearity in the governing equations, application of this simulation code to other sets of properties cannot be guaranteed. Hence to ascertain versatality of the present formulation and computer code, simulation should be performed with other variants of the formation

(2) **Three-phase flow:**

In addition to oil and water, the third phase present in certain reservoirs is air, though comparatively much less in quantity A three phase simulation of oil, water and air would thus lend more credibility to this work Also we can take up the three phase simulation of oil, water and steam for the future analysis

(3) **Adsorption-Desorption in the formation:**

In the case of surfactant flooding, we can take into account the adsorption-desorption phenomena, i.e transfer of surfactants from the injected flow to the formation and vice versa respevtively The mass transfer phenomena will obviously call for modification in the constitutive relations in conjunction with the variation of concentration of the surfactant solution It will lead to the inclusion of an additional mass transfer equation that must be solved along with the pressure equations

(4) **Enhancement in the two-spot problem:**

In case of the two-spot problem, we can consider the original two-spot model (Figure 2 2 (b)), in stead of the simplified flow domains (Figures 2 2 (c), (d) and (e)) Obviously, it will include variable grid and proper handling of the boundary conditions on the circular arc shaped injection and production zones. It will invariably make the problem computationally more intensive Enhancement of this problem for non-isothermal case is also highly recommended for further analysis. It will invoke an additional energy equation which must be solved along with the pressure equations, thus making the problem much more computation expensive Also we know that in the vicinity of the injection and production wells, near-field effects are predominant. Therefore, we can extend the domain decomposition technique by localizing the affected regions through assigning separate subdomains to them and studying them closely

(5) **Three dimensional simulation:**

An extension of the present work for the rectangular flow domain can be a three dimensional simulation including inhomogeneity and anisotropy of the formation This will also make the reservoir simulation computationally more expensive. Domain decomposition with parallelization can be a very good option for this problem.

(6) **Interface treatment:**

In the domain decomposition problem, Uzawa's algorithm should be looked into much more details for the interface treatment In this regard, matching of the mass fluxes instead of the pressure gradients at the interface, is highly recommended Also we can go for some advanced parallelizable techniques (Glowinski, 1983), in lieu of the Uzawa's algorithm which can be expectecd to enhance the convergence rate of interface iterations and make the entire simulation faster

(7) **Parallelization:**

The major task recommended for future extension is to parallelize the code developed for the domain decomposition problem. The successful implementation would not only save a lot of computational time but also enable us to perform real life reservoir simulation problems.

References

[1] Aziz, K (1983), Modelling of Thermal Oil Recovery Processes, *Mathematical and Computational Methods in Siesmic Exploration and Reservoir Modelling*, SIAM, Philadelphia

[2] Boberg, T C (1988), *Thermal Methods of Oil Recovery*, An Exxon Monograph, John Willey, New york

[3] Barenblatt, G. I., Entov, V. M. and Ryzhik, V. M (1990), *Theory of Fluid Flows Through Natural Rocks*, Kluwer, Dordrecht

[4] Chatterjee, A. and Muralidhar, K. (1995), Numerical Study of Enhanced Oil Recovery Using Surfactants, *International Journal for Heat and Fluid Flow*, Vol. 5, No 4

[5] Duff, I. S. (1980), *MA28-A Set of Fortran Subroutines for Sparse Unsymmetric Linear Equations*, AERE Harwell.

[6] Ewing, R. E (Ed.) (1983), *Mathematics of Reservoir Simulation*, SIAM, Philadelphia

[7] Glowinski, R., Dinh, Q V and Periaux J. (1983), Domain Decomposition Methods for Non-linear Problems in Fluid Dynamics, *Computational Methods in Applied Mechanics and Engineering*, Vol 40

[8] Golub, G H and O'leary, D P. (1989), Some History of the Conjugate and Lanczos Algorithms 1948 - 1976, *SIAM Review*, Vol. 31, No 1, 50-102.

[9] Hackbusch, W (1992), A Parallel Conjugate Gradient Method, *Journal of Numerical Linear Algebra with Applications*, Vol 1, No 2, 122-147.

[10] Le Tallec, P (1994), Domain Decomposition Methods in Computational Mechanics, *Computaional Mechanics Adv* , 1(2), 121-220.

[11] Muralidhar, K and Sundararajan, T. (Ed) (1995), *Computational Fluid Flow and Heat Transfer*, Narosa Publishing House, India

[12] Muralidhar, K , Chatterjee, A and Nagabhusana Rao, B. V. (1996), Application of Domain Decomposition in Modelling Flow and Heat Transfer Problems, *IMechE*, Vol 210

[13] Muralidhar, K , Verghese, M , Pillai, K M (1993), Application of an Operator Splitting Algorithm for Advection-Diffusion Problems, *Numerical Heat Transfer*, Vol 23, 99-113.

[14] Perng, C. Y. and Street, R. L (1991), A Coupled Multigrid-domain Splitting Technique for Simulating Incompressible Flows in Geometrically Complex Domains *International Journal of Numerical Methods in Fluids*, 18, 269-286

[15] Pillai, K M and Muralidhar, K (1993), A Numerical Study of Oil Recovery Using Water Injection Method, *Numerical Heat Transfer,* (A) 24, 305-322

[16] Pruess, K. and Narasimhan, T. N. (1982), On Fluid Reserves and the Production of Superheated Steam from Fractured, Vapour-dominated Reservoirs, *Journal of Geophysical Research*, Vol 87, 9329–9339.

[17] Shah, D. O. and Schechter, R. S. (1977), *Improved Oil Recovery by Surfactant and Polymer Flooding*, Academic Press.

[18] Sorbie, K. S , Zhang, H. R. and Tsibuklis, N B (1995), Linear Viscous Fingering New Experimental Results, Direct Simulation and the Evaluation of Averaged Models, *Chemical engineering Science*, Vol. 51, 601-616

[19] Stevenson, M D., Kagan, M and Pinczewski, V. W. (1991), Computational Methods in Petroleum Reservoir Simulation, *Computers in Fluids,* Vol. 19, No. 1-19.

[20] Uren, L C and Fahmy, E. H (1972), *Factors Influencing the Recovery of Petroleum from Unconsolidated Sands by Water flooding*, AIME, Vol.318.

[21] Zhang, H. R , Sorbie, K S. and Tsibuklis, N B. (1997), Viscous Fingering in Five-spot Experimental Porous Media: New Experimental Results and Numerical Simulation, *Chemical Engineering Science,* Vol 52, No 1, 37-54

Appendix A

Table A.1 Fluid and Formation Properties

K	132 darcies
K_h	0 1661 W/m °C
ϵ	0 375
ξ_o	0 03447 Pa^{-1}
ξ_w	0 02137 Pa^{-1}
β_o	2 28 $\times$ 10^{-4} $°C^{-1}$
β_w	2 28 $\times$ 10^{-4} $°C^{-1}$
c_o	2092 (J/kg-°C)
c_w	4184 (J/kg-°C)
$(\rho c)_R$	2413 (J/m^3-°C)
ρ_o	90% of ρ_w

Table A 2 Oil and Water Viscosities

T, °C	20	40	60	80
μ_o, Pa-s	4.12	2.37	0.61	0.10
μ_w, Pa-s	1.03 $\times$ 10^{-4}	6.6 $\times$ 10^{-4}	4 73 $\times$ 10^{-4}	3.67 $\times$ 10^{-4}

Table A.3. Constitutive Relations

S_w	k_{rw}	k_{ro}	$p_{c_{ow}}$, KPa
0 1*	0	1.0	28.34
0 2	0.0016	0 875	0 655
0.3	0 0081	0.735	0 496
0 4	0 0259	0 590	0 4205
0.5	0 0672	0.420	0.352
0 6	0.1000	0.210	0 283
0.7	0 1400	0 070	0 214
0 8	0 2000	0.016	0.145
0 86†	0 2500	0	0 0758

* Irreducible limit for water

† Irreducible limit for oil